

**EXPERIMENTAL CONTRIBUTION ANALYSIS OF EXTERNAL NOISE
COMPONENTS TO THE INTERIOR NOISE OF AN AUTOMOBILE**

A Thesis

by

SEONGIL HWANG

Submitted to the Office of Graduate and Professional Studies of
Texas A&M University
in partial fulfillment of the requirements for the degree of

MASTER OF SCIENCE

Chair of Committee, Yong-Joe Kim
Committee Members, Edward B. White
Luis San Andres

Head of Department, Andreas A. Polycarpou

December 2016

Major Subject: Mechanical Engineering

Copyright 2016 Seongil Hwang

ABSTRACT

The contribution analysis of various noise sources in the automobile interior noise is important for a well-designed vehicle with a low interior noise level. The proposed modified Cholesky Decomposition (CD) is able to decompose the interior noise spectra into multiple spectra, each physically representing the contribution of a specific noise source to the interior noise of the automobile. During an experiment with two speakers driven by two independent white noise signals, it is shown that the measured noise spectrum can be successfully decomposed into two contributions, each associated with noise radiated from speakers.

Then, a simplified, scaled automobile model (with one side mirror, one front and two side windows, and flat top, back, and bottom panels) was tested in a wind tunnel at the airflow speeds of 15 m/s (54 km/h) and 24 m/s (86.4 km/h). In this experiment, 14 external and 1 interior microphones were implemented to measure the external aeroacoustic source signals and the interior noise signal respectively. The results obtained by processing the microphone signals reveal the contributions of the external aeroacoustic noise sources to the interior noise.

In addition, an automobile was tested on a road at the speeds of 104.6 km/h (65 mph, or 29.1 m/s) and 128.7 km/h (80 mph, or 35.8 m/s). In this experiment, 64 exterior and 4 interior microphones measured the external noise source signals and interior noise signals, respectively. The results obtained by processing the measured microphone signals indicated the highest contributor of the external aeroacoustic noises are the windows and the hood. It was also detected that the contribution of the windows

increased as the speed increased and the highest contribution of the interior noise occurred to the seat closer to the window.

The proposed CD-based procedure requires installing microphones flush-mounted on the exterior surface of the automobile to measure the noise source signals. However, the surface-flush-mounted microphone installation can be labor-intensive and time-consuming, making it difficult to evaluate a large number of aeroacoustic design cases. Thus, an innovative, CD-based contribution analysis system integrated with an exterior microphone array is proposed. In this integrated system, the surface-flush-mounted microphones are replaced with the exterior microphone arrays. This array-measurement-based contribution analysis procedure was validated by conducting an experiment with two speakers and an 8 by 8 array of microphones.

TABLE OF CONTENTS

	Page
ABSTRACT	ii
TABLE OF CONTENTS	iv
LIST OF FIGURES.....	vi
LIST OF TABLES	ix
1. INTRODUCTION.....	1
2. CD-BASED CONTRIBUTION ANALYSIS THEORY	6
3. EXPERIMENT WITH TWO SPEAKERS	11
3.1 Experimental Setup	11
3.2 Results and Discussion.....	12
4. EXPERIMENT WITH SIMPLIFIED, SCALED AUTOMOBILE MODEL.....	16
4.1 Design Overview.....	16
4.2 Outer Plates	17
4.3 Interior Noise Insulation Materials	18
4.4 Windows (Glasses).....	18
4.5 Side Mirror and Rain Gutters	18
4.6 Supports for Model.....	19
4.7 Microphone Fairings	19
5. WIND TUNNEL TEST AND RESULTS	21
5.1 Klebanoff-Saric Wind Tunnel.....	21
5.2 Experimental Setup for Wind Tunnel Test	21
5.3 Wind Tunnel Test.....	23
5.4 Test Results and Discussion.....	25
6. EXPERIMENT WITH AUTOMOBILE AND RESULTS.....	31
6.1 Experimental Setup for Automobile Test.....	31
6.2 Test Results and Discussion.....	35
7. MICROPHONE-ARRAY-MEASUREMENT-BASED CONTRIBUTION ANALYSIS	40

7.1 Identification of Source Locations Using Two Beamforming Methods	41
7.2 Reconstruction of Virtual Source Signals from Measured Array Signals	42
7.3 Experimental Setup for Validation.....	43
7.4 Test Results and Discussions	45
8. CONCLUSIONS.....	50
REFERENCES	52
APPENDIX	57
A. Contribution Analysis Software	57
A.1 Description of CAS	58
A.2 Quick instruction.	64

LIST OF FIGURES

	Page
Figure 1: Overall signal processing procedure.....	9
Figure 2: Experimental setup with two speakers: (a) Schematic diagram of equipment connection and (b) Locations of speakers and microphones, and speaker excitation signals.	11
Figure 3: Contribution results with two speaker data: (a) Contribution in percent, (b) Group contribution in percent, (c) Contribution in dB, and (d) Contribution in 1/3 octave dBA.	13
Figure 4: Contribution results with two speaker data: (a) SVD-based contribution, (b) CD-based contribution.....	15
Figure 5: Simplified, scaled automobile model.	16
Figure 6: (a) Supports of model and their covers, (b) Side view of cover, and (c) Bottom view of cover.	19
Figure 7: (a) 3-D printed microphone fairing and (b) Assembled with microphone.	20
Figure 8: Microphone locations in automobile model: (a) Left side view and (b) Top view.....	22
Figure 9: Wind tunnel test results at airflow speed of 24 m/s without interior noise treatment in frequency range up to 4 kHz. (a) Auto-spectrum of interior microphone in both wind tunnel test and interior acoustic resonance test and (b) Multiple coherence between exterior and interior microphone signals in wind tunnel test.....	26
Figure 10: Comparison of auto-spectra measured by using exterior and interior microphones in 4 test configurations. (a) 15 m/s with interior noise treatment, (b) 24 m/s with interior noise treatment, (c) 15 m/s without interior noise treatment, and (d) 24 m/s without interior noise treatment.	26
Figure 11: Results of wind tunnel test at flow speed of 24 m/s without interior noise treatment and interior resonance test without both airflow and interior noise treatment. (a) Auto-spectrum of interior microphone, (b) Multiple coherence between exterior and interior microphone signals, and (c) Interior auto-spectrum decomposed by using normalized contribution.	27

Figure 12: Zoomed contribution results: (a) 164 Hz, (b) 205 Hz, (c) 364 Hz, (d) 498 Hz, and (e) 669 Hz.....	29
Figure 13: Zoomed contribution results: (a) 736 Hz, (b) 803 Hz, (c) 817 Hz, (d) 878 Hz, and (e) 965 Hz.....	30
Figure 14: Experimental setup with automobile: (a) Schematic of equipment connection and (b) Equipment inside automobile’s trunk.....	31
Figure 15: Microphone installation locations. Refer to Table 9 for the description of the microphone locations.....	31
Figure 16: Locations of grouped microphones. Refer to Table 10 for the description of the microphone groups.....	32
Figure 17: 1/3 octave band contributions of microphone groups (Figure 16 and Table 10) to interior noise at front driver side seat in dBA at automobile speed of 80 mph.....	36
Figure 18: Overall contribution results of microphone groups (Figure 16 and Table 10) to interior noise at front driver side seat at speed of 80 mph.....	37
Figure 19: Effects of automobile speeds on overall contribution of microphone groups (Figure 16 and Table 10) at front driver side seat.....	38
Figure 20: Effects of seat positions on overall contribution of microphone groups (Figure 16 and Table 10) at automobile speed of 80 mph.....	39
Figure 21: Scheme of beamforming based contribution analysis.....	40
Figure 22: Experimental setup for validation of beamforming with microphone array and CD-based contribution analysis procedure: (a) Illustration of experimental setup, (b) Three speakers with the nine reference microphones, and (c) the microphone array and receiver microphone placed at the center of the array.....	44
Figure 23: DAS beamforming powers on the front of the three speakers at different frequencies: (a) 1 kHz, (b) 1.5 kHz, (c) 2 kHz, (d) 2.5 kHz, (e) 3 kHz, (f) 3.5 kHz, (g) 4 kHz, (h) 4.5 kHz, and (i) 5 kHz. Notes that white lines in the plot show the locations of the speakers, and speaker units.....	46
Figure 24: MUSIC beamforming powers on the front of the three speakers at different frequencies: (a) 1 kHz, (b) 1.5 kHz, (c) 2 kHz, (d) 2.5 kHz, (e) 3 kHz, (f) 3.5 kHz, (g) 4 kHz, (h) 4.5 kHz, and (i) 5 kHz. Notes that white lines in the plot show the locations of the speakers, and speaker units.....	48

Figure 25: Contribution analysis results obtained with real and virtual source signals:
(a) Real source signals measured by using real reference microphones and
(b) Virtual source signals reconstructed by using measured array
microphone signals.49

LIST OF TABLES

	Page
Table 1: Three layers of interior noise insulation materials.....	18
Table 2: Information on Klebanoff-Saric Wind Tunnel (KSWT) [26] at Texas A&M University.	21
Table 3: Exterior microphone locations (Refer to Figure 8).....	22
Table 4: Configurations of wind tunnel test and interior acoustic resonance test.....	23
Table 5: Two airflow speeds of KSWT and BPFs of fan at two speeds.	24
Table 6: Frequency range of vortex shedding caused by side mirror.	24
Table 7: First three highest contributions at selected interior noise peak frequencies in Figure 12.....	29
Table 8: First three highest contributions at selected interior noise peak frequencies in Figure 13.....	30
Table 9: List of noise source microphone locations (Refer to Figure 15).....	33
Table 10: Grouping of noise source microphones (Refer to Figure 16).	34

1. INTRODUCTION*

To design an automobile with low-level interior noise, it is important to analyze the contribution of various noise sources to the interior noise. Once the contribution of the noise sources is identified, noise control strategies can be developed based on the impacts of the noise sources. In general, a noise source with a highest contribution is targeted foremost, to reduce the overall interior noise level. Here, a novel contribution analysis technique based on the Cholesky Decomposition (CD) is proposed to decompose the auto-spectrum of the interior noise into multiple auto-spectra, as a function of frequency, of which each spectrum, uncorrelated with other spectra, represents the contribution of a specific noise source to the interior noise. This contribution analysis can result in physically meaningful decomposition of the interior noise in association with physical noise sources.

In an automobile, noise is mainly generated from structure-borne and air-borne noise sources. The structure-borne noises are mainly generated from the structural vibration, (e.g., of the engine, the transmission, the road/tire). The air-borne noises can be generated from aerodynamic excitations [1]. As structure-borne noise mitigation techniques, (e.g., for noise insulation, engine tuning and mounting, and active vibration control), have been significantly advanced and automobile speed limits have been increased, exterior aeroacoustic noise sources became critically important as major

* Parts of this section are reprinted from “Experimental contribution analysis of external aeroacoustic noise components to interior noise of simplified, scaled automobile model in wind tunnel” by Seongil Hwang, Myunghan Lee, Kang Duck Ih, Edward B. White, and Yong-Joe Kim, 2016, *Proceedings of Noise-Con 2016, Providence, RI, United States*, Copyright [2016] with permission by NoiseCon 2016 of INCE-USA.

contributors to the interior noise. Although the proposed method can be used to analyze the contribution of any structure-borne and air-borne noise sources, this article focuses on the aeroacoustic noise sources due to their high contributions to the interior noise of modern automobiles.

Tcherniak and Schuhmacher [2] summarized existing analysis methods, to estimate the contributions of automotive noise, vibration, and harshness (NVH) sources, classifying them into two categories, synthesis and decomposition approaches, based on how to identify source strengths. One of the most widely-used synthesis approaches is the Transfer Path Analysis (TPA) [3-4]. The decomposition approaches include the Multiple Coherence method [5-6], the Operation Transfer Path Analysis (OTPA) [7-13], and the Transmissibility Matrix Method (TMM) [14-21].

The classical TPA, also known as the Source Path Contribution (SPC) or the Noise Path Analysis (NPA), requires the measurement of Frequency Response Functions (FRFs) to determine Transfer Functions (TFs) between input and output points (i.e., reference and receiver points) by using impact hammers or shakers for structure-borne paths or loudspeakers for air-borne paths. Then, synthesized output signals can be calculated by estimating source strength at each input point and combining the estimated source strength with the measured FRFs [7]. The limitations of the conventional TPA are the time-consuming measurement process to obtain the TFs and the errors induced by the estimated source strengths.

The OTPA first requires experimental data, e.g., interior noise signals and noise source signals, under operational conditions and measured or estimated TFs in isolated

conditions of which each condition has only one source turned on [8-9]. Then, a Principle Component Analysis (PCA) technique such as the Singular Value Decomposition (SVD) can be applied to decompose operational source strengths from the operational data. The operational source strengths can be combined the isolated TFs to identify the contributions of the sources [8]. The OTPA can be used to address the main drawbacks of the classical TPA such as the time-consuming measurement process and the errors induced by the estimated source strengths [2, 10]. However, the conventional OTPA has the drawback of cross-coupling (or cross talk) between sources, which can result in incorrect contribution results. This drawback has been overcome by using a PCA such as the SVD for the Cross-Talk Cancellation (CTC) [11-13].

The concept of transmissibility was introduced first in two papers in 1988, one by Liu and Ewins [14] and the other by Varato and McConnell [15]. In the same year, the transmissibility matrix, also known as the Acoustic Transfer Function (ATF) between two measured responses, was defined by Riberio [16]. The Transmissibility Matrix Method (TMM) made it possible not to measure the time-consuming measurement of the TFs for the contribution analysis: only operational data was required for it. Further investigation to improve the accuracy and applicability of the TMM was made by Maia, Fontul, and Tcherniak [17-21]. Although the current state-of-the-art approaches based on the TMM and the SVD require only operational data to estimate the contributions of noise sources, it is still difficult to identify the contributions related to physically-meaningful sources since the SVD decomposes purely mathematical sources.

A noise signal measured inside or outside an automobile can include multiple noise source components: for example, a microphone mounted on an engine hood can measure both aeroacoustic noise and engine noise. The proposed approach can be used to decompose the measured noise signals into independent noise sources (in the latter example, the aeroacoustic noise source and the engine noise source) and calculate the virtual ATFs from the decomposed independent noise sources to interior noise measurement points to analyze the contribution of each independent source to the interior noise.

While the concept of the sound field decomposition [22-23] already exists mostly for structure-borne noise, the decomposition of aeroacoustic noise and the calculation of the virtual ATFs have been barely investigated before. In addition, a procedure to identify the contributions of physically meaningful noise sources to specific receiver points do not exist. The proposed approach is a Multiple-Input and Multiple-Output (MIMO) procedure, while existing ATF calculation or measurement procedures are mostly based on the Single-Input and Single-Out (SISO) assumption. Thus, the existing SISO ATF approaches can result in large errors when they are applied to predict the interior noise levels or contributions of multiple noise sources in an automobile that is a MIMO system.

The proposed technique was verified by conducting experiments with two speakers. The contribution analysis of the experimental data shows that the contribution of each speaker can be successfully decomposed from measured microphone signals. In addition to these simple speaker experiments, a simplified, scaled automobile model was

built and tested in a wind tunnel at two airflow speeds of 15 m/s and 24 m/s to analyze the contributions of external aeroacoustic noise sources to the interior noise. Lastly, an automobile was tested at two different speeds of 65 miles per hour (mph) and 80 mph to analyze the contributions of the automobile's exterior noise sources to the interior noise.

2. CD-BASED CONTRIBUTION ANALYSIS THEORY*

The proposed contribution analysis approach is an experimental method, requiring the measurement of multiple noise source signals simultaneously with interior noise signals. The signals of external aeroacoustic noise sources can be measured on the exterior surface of an automobile by placing flush-mounted microphones or surface microphones with fairings in specific aeroacoustic source areas, e.g., the side mirrors, the pillars, the wind shield, etc. Other external noise source signals can be measured by using various transducers such microphones and accelerometers.

In the measurement, any two source signals measured by using two adjacent microphones need to be weakly correlated or uncorrelated to minimize the total number of microphones. The latter condition can be achieved by placing the two microphones at a distance larger than the turbulence coherence length. This condition can be also achieved by increasing the distance between the two microphones until the coherence function of the two measured signals is much lower than 1. The total number of the source signals can be determined to satisfy that the multiple coherence function between the source signals and one of the interior noise signals is close to 1. When the multiple coherence function is lower than 1, the number of the source microphones needs to be increased.

* Parts of this section are reprinted from “Experimental contribution analysis of external aeroacoustic noise components to interior noise of simplified, scaled automobile model in wind tunnel” by Seongil Hwang, Myunghan Lee, Kang Duck Ih, Edward B. White, and Yong-Joe Kim, 2016, *Proceedings of Noise-Con 2016, Providence, RI, United States*, Copyright [2016] with permission by NoiseCon 2016 of INCE-USA.

When N noise source signals represented by a column vector of \mathbf{s} and M interior noise signals of \mathbf{p} are measured simultaneously, an ATF matrix can be used to relate the vectors of these signals in a frequency domain as

$$\mathbf{p} = \mathbf{H}\mathbf{s}, \quad (1)$$

where \mathbf{H} is the M by N ATF matrix of which the (i, j) element is the ATF between the i -th interior noise signal and the j -th noise source signal. Then, the auto-spectra of the interior noise signals can be represented as

$$\mathbf{S}_{pp} = \mathbf{E}(\mathbf{p}\mathbf{p}^H) = \mathbf{H}\mathbf{E}(\mathbf{s}\mathbf{s}^H)\mathbf{H}^H = \mathbf{H}\mathbf{S}_{ss}\mathbf{H}^H, \quad (2)$$

where “E” represent the ensemble average, the superscript, “H” represents the Hermitian operator, and \mathbf{S}_{ss} is the cross-spectral matrix of the source signals. The cross-spectral matrix of the source signals can be decomposed by using a modified CD into

$$\mathbf{S}_{ss} = \mathbf{L}\mathbf{D}\mathbf{L}^H, \quad (3)$$

where \mathbf{L} is the lower triangular matrix and \mathbf{D} is the diagonal matrix of which each element represents the auto-spectrum of an independent source signal. In the CD process, the cross-spectral matrix is diagonalized without changing the order of the original diagonal elements (i.e., the auto-spectra of the measured noise source signals) as pivots. Thus, each diagonal element in \mathbf{D} of Eq. (3) can be directly related to a source signal, although a diagonal matrix, obtained by using other mathematical decomposition approach such as the Singular Value Decomposition (SVD), is difficult to be related to physical sources due the order change of the diagonal elements. Then, the contribution of the i -th independent source to the interior noise auto-spectra can be presented as

$$\mathbf{S}_{pp_i} = \text{diag} \left\{ \mathbf{H}\mathbf{L} [d_i] \mathbf{L}^H \mathbf{H}^H \right\}, \quad (4)$$

where “diag” represents the diagonal matrix, $[d_i]$ is a diagonal matrix of which all the elements are zero except that the i -th element is the same as the i -th element of \mathbf{D} . Here, the virtual ATF of the i -th independent source signal to the interior noise signals is then represented by

$$\mathbf{H}\mathbf{v}_i = \mathbf{H}\mathbf{L} [1_i], \quad (5)$$

where $[1_i]$ is a diagonal matrix of which all the elements are zero except that the i -th element is 1. The contribution in Eq. (4) can be normalized as

$$\mathbf{C}_i = \mathbf{S}_{pp_i} \cdot / \text{diag}(\mathbf{S}_{pp}), \quad (6)$$

where \mathbf{C}_i is the normalized contribution of the i -th source with the range of 0 to 1 and the symbol, “./” represents the element-by-element division.

The contribution in an octave or 1/3 octave band can be expressed by the summation of the contributions, in the entire linear frequency range, obtained by applying the octave or 1/3 octave band pass filter to the time data. This band synthesis procedure can be represented as

$$\mathbf{C}_{\text{octave}} = \frac{\sum_{nf=1}^{N_f} (\mathbf{C}_{nf} \cdot \mathbf{S}_{pp,nf})}{\sum_{nf=1}^{N_f} \mathbf{S}_{pp,nf}}, \quad (7)$$

where N_f is the number of the linear frequency lines. The overall contribution is then calculated by the summation of the contributions in the entire octave or 1/3 octave frequency bands as

$$\mathbf{C}_{\text{overall}} = \frac{\sum_{nb=1}^{N_b} (\mathbf{C}_{\text{octave},nb} \cdot \mathbf{s}_{pp,nb})}{\sum_{nb=1}^{N_b} \mathbf{s}_{pp,nb}}, \quad (8)$$

where N_b is the number of the entire octave or 1/3 octave frequency bands. A single contribution of grouped, multiple, measured source signals (i.e., a group contribution) can be obtained by the summation of the normalized contributions of all the noise source signals in this group as

$$\mathbf{C}_{\text{group}} = \mathbf{C}_1 + \mathbf{C}_2 + \dots + \mathbf{C}_{N_g}, \quad (9)$$

where N_g is the number of the source signals in the group.

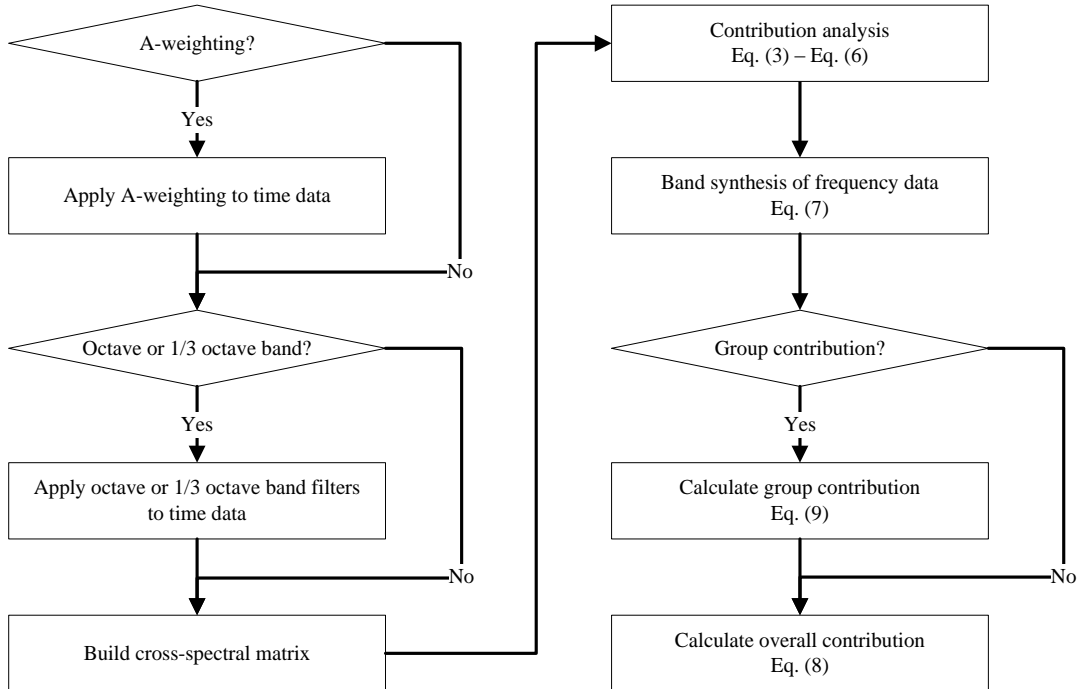


Figure 1: Overall signal processing procedure.

The overall signal processing procedure is shown in Figure 1. In this procedure, it is assumed that time data is obtained from exterior and interior sensors connected to a data acquisition system. If needed, the A-weighting is applied to the time data and octave or 1/3 octave band pass filters are applied to the time signals to obtain the contribution analysis results in octave or 1/3 octave bands. The cross-spectral matrices are then built by applying the Fast Fourier Transformation (FFT) to the time-windowed data and by averaging the spectra linearly. The contribution of each source to each receiver is obtained from Eqs. (3) to (6) and the frequency data in each octave or 1/3 octave band is obtained by using the linear band summation in Eq. (7). The overall contribution can be calculated by using Eq. (8).

3. EXPERIMENT WITH TWO SPEAKERS*

3.1 Experimental Setup

For the validation of the proposed contribution analysis method, an experiment with two speakers and five microphones was conducted as shown in Figure 2. The first four microphones can be assumed as the reference microphones to measure the noise source signals and the last microphone (microphone 5), as the receiver (or interior) microphone.

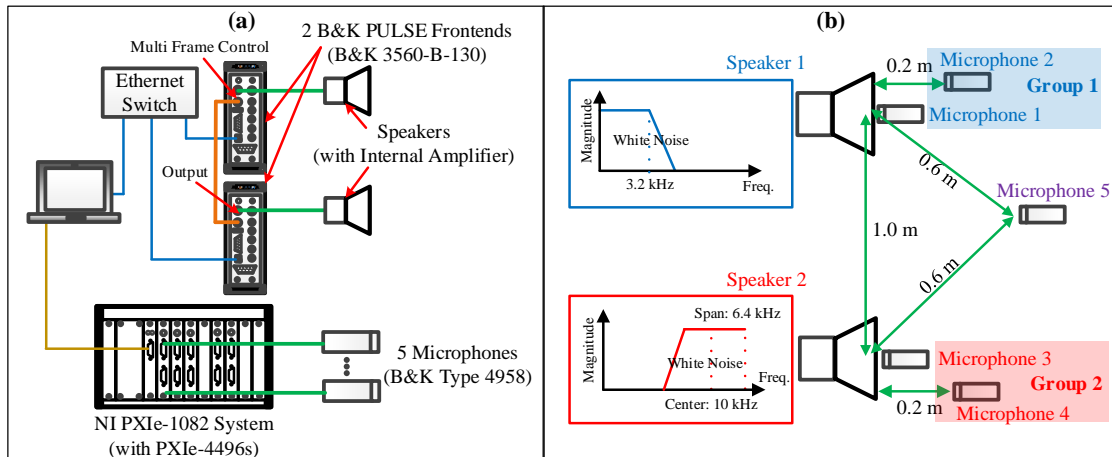


Figure 2: Experimental setup with two speakers: (a) Schematic diagram of equipment connection and (b) Locations of speakers and microphones, and speaker excitation signals.

The filtered white noise signals, generated from the two signal generators in two synchronized 3560-B-130 Brüel & Kjær (B&K) PULSE systems, were used to drive the

* Parts of this section are reprinted from “Experimental contribution analysis of external aeroacoustic noise components to interior noise of simplified, scaled automobile model in wind tunnel” by Seongil Hwang, Myunghan Lee, Kang Duck Ih, Edward B. White, and Yong-Joe Kim, 2016, *Proceedings of Noise-Con 2016, Providence, RI, United States*, Copyright [2016] with permission by NoiseCon 2016 of INCE-USA.

two speakers independently. The first excitation signal to drive speaker 1 is a low-pass-filtered, white noise with the cut-off frequency of 3.2 kHz. The other excitation signal for speaker 2 is a band-pass-filtered, white noise with the center frequency of 10 kHz and the frequency span of 6.4 kHz.

The acoustic pressure signals were measured by connecting the microphones to a National Instrument (NI) PXIe-1082 chassis with data acquisition modules of NI PXIe-4496. An in-house NI LabVIEW code was built and used to acquire the microphone time data at a sampling rate of 20 kHz for 120 seconds. The acquired time data was processed by using an in-house MATLAB code to obtain the contributions of the reference microphone signals to the receiver microphone signal.

3.2 Results and Discussion

Figure 3 shows the contribution analysis results of the experiment with the two speakers. The normalized contributions, in Eq. (6), of the reference microphone signals to the receiver microphone signal are presented in Figure 3(a). The total contribution obtained by adding all the four normalized contributions at each frequency represents the multiple coherence function in percent: i.e., the total contribution divided by 100 represents the multiple coherence function in the range of 0 to 1. The multiple coherence function between the signals of the receiver microphone (i.e., microphone 5) and the reference microphones (i.e., microphones 1 to 4) in the entire frequency range is mostly higher than 0.8. This indicates that the contribution of the reference microphone signal to the receiver microphone signal in this frequency range is dominant, resulting in meaningful contribution data.

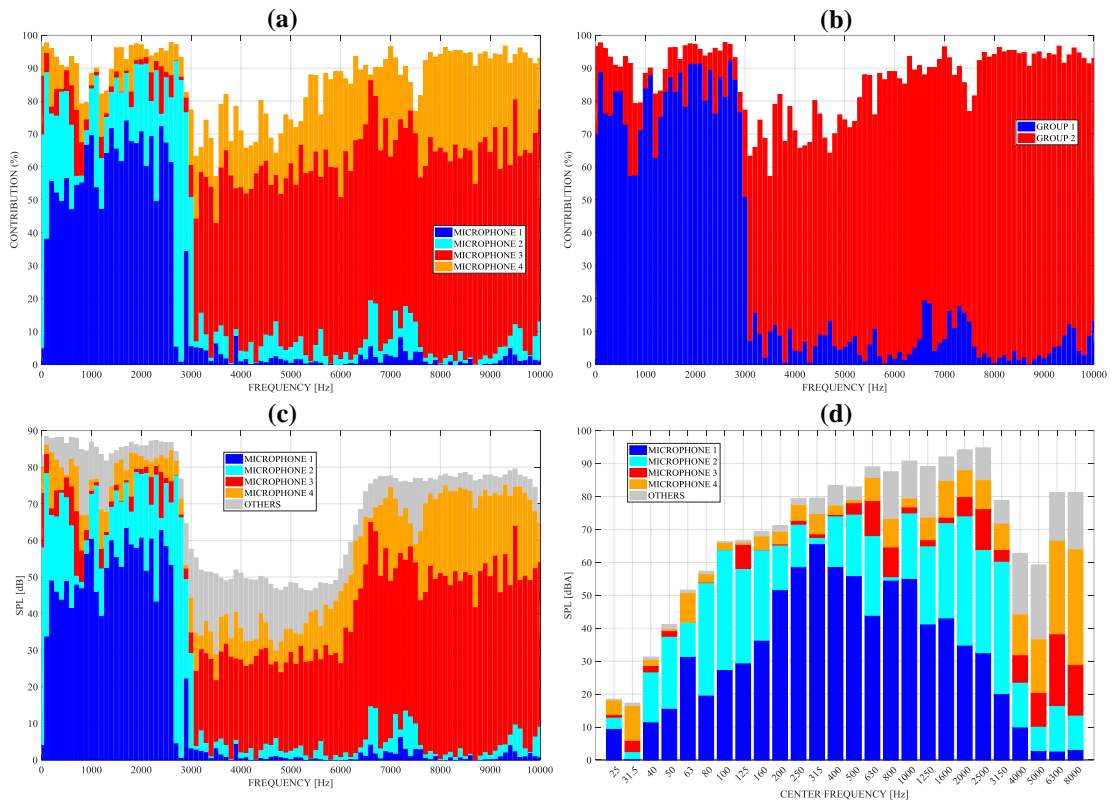


Figure 3: Contribution results with two speaker data: (a) Contribution in percent, (b) Group contribution in percent, (c) Contribution in dB, and (d) Contribution in 1/3 octave dBA.

The contribution analysis results in Figure 3(a) indicate that the microphone 1 and 2 signals are dominantly contributing to the auto-spectrum of microphone 5 in the low frequency range up to 3.2 kHz. In the high frequency range of 6.8 kHz to 10 kHz, the microphone 3 and 4 signals are most influential to the auto-spectrum of microphone 5.

The group contribution results calculated by using Eq. (9) are shown in Figure 3(b). Group 1 was including the acoustic pressure signals of microphones 1 and 2 placed in front of speaker 1 as shown in Figure 2(b), and the signals of microphones 3

and 4 located closer to speaker 2 were grouped as group 2. In the low frequency range, up to 3.2 kHz, mainly excited by speaker 1, group 1 is dominant in the contribution results, and in the high frequency range, above 6.8 kHz, dominantly excited by speaker 2, group 2 is significant.

The linearly scaled contribution in dB, introduced for the convenience to interpret the contribution analysis results, is shown in Figure 3(c). This contribution is calculated by linearly combining the contribution results in percent and the auto-spectrum of the receiver microphone. For example, 42 % contribution of 90 dB at 100 Hz in Figure 3(c) is represented as 37.8 dB that is obtained by multiplying 0.42 and 90 dB. The gray colored contribution labeled as "Others" in Figure 3(c) and Figure 3(d) represents a contribution of other sound sources (e.g., background noise) that are not measured with the reference microphones.

In Figure 3(c), the total contribution obtained by linearly adding all the five contributions (i.e., the four reference microphone contributions and the "other" contribution) in dB represents the auto-spectrum of the receiver microphone signal. In the low frequency range up to 3.2 kHz, the auto-spectra of microphones 1 and 2 are approximately 10 to 30 dB higher than the others, since these two microphones are placed closer to speaker 1 than the others. In the high frequency range of 6 kHz to 10 kHz, the auto-spectra of microphones 3 and 4 are approximately 10 to 40 dB higher than the others due to their proximity to speaker 2. Finally, the contributions in 1/3 octave bands are shown in Figure 3(d).

Figure 4 shows the comparison of the SVD- and CD-based contributions between by using SVD shown in Figure 4 (a) and by using CD shown in Figure 4 (b). The SVD based contribution is hard to identify the measured channels although it looks very similar with CD based contributions of microphones 1 and 2 at the low frequencies can be associated with the sound radiation from speaker 1 since microphones 1 and 2 are placed close to speaker 1 and the contribution results at the high frequencies can be related to the sound radiation from speaker 2.

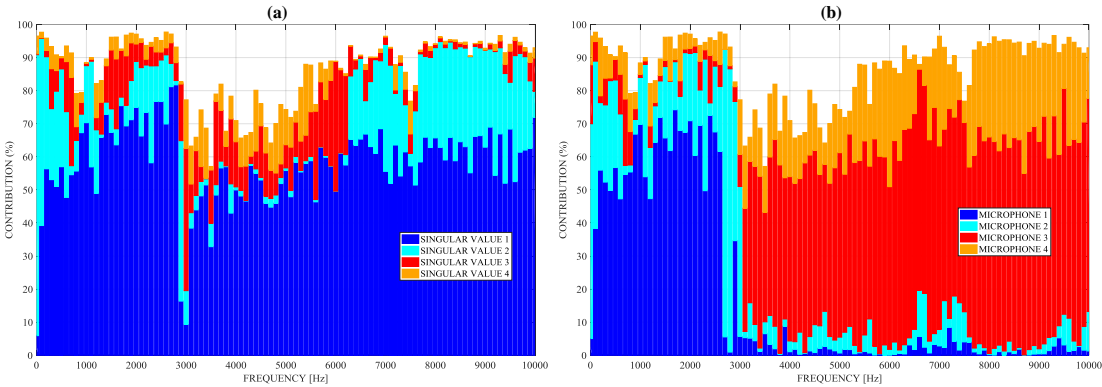


Figure 4: Contribution results with two speaker data: (a) SVD-based contribution, (b) CD-based contribution.

4. EXPERIMENT WITH SIMPLIFIED, SCALED AUTOMOBILE MODEL*

4.1 Design Overview

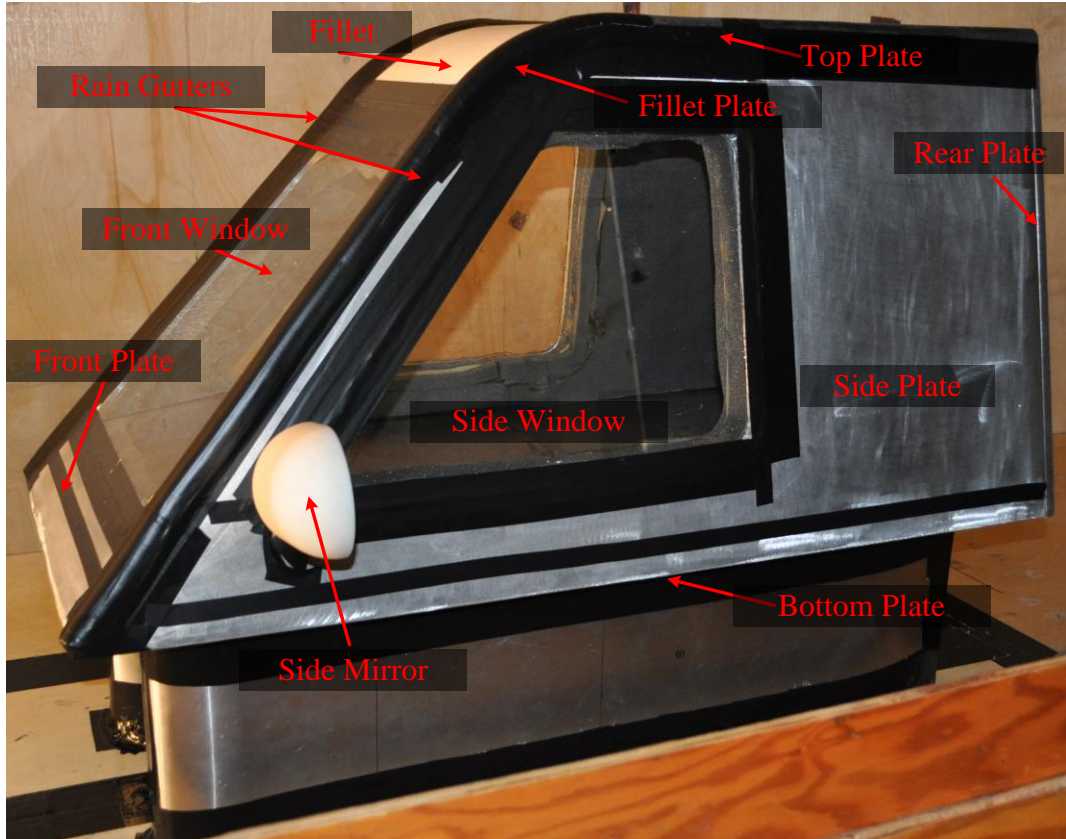


Figure 5: Simplified, scaled automobile model.

A simplified automobile model was designed based on the Hyundai Simplified Model (HSM) [24] and scaled down to fit the test section of the Klebanoff-Saric Wind Tunnel (KSWT) at Texas A&M University as shown in Figure 5. This simplified,

* Parts of this section are reprinted from “Experimental contribution analysis of external aeroacoustic noise components to interior noise of simplified, scaled automobile model in wind tunnel” by Seongil Hwang, Myunghan Lee, Kang Duck Ih, Edward B. White, and Yong-Joe Kim, 2016, *Proceedings of Noise-Con 2016, Providence, RI, United States*, Copyright [2016] with permission by NoiseCon 2016 of INCE-USA.

scaled model consists of seven plates, three windows, one side mirror, one round fillet, two rain gutters, and interior noise treatment materials. The outer width, height, and length are 19.7 inch, 19.7 inch, and 39.4 inch, respectively. The front and the two side plates are inclined at the angles of 40° and 10° respectively from the vertical line. All the length units in this article are in inch unless specified otherwise.

The front and side windows were installed into the outsides of the front and side plates by using silicon glue. The side mirror was assembled into the side plate with three bolts from the outside. The rain gutters are attached along the top lines of the side plates.

4.2 Outer Plates

$7/16''$ thick MIC6 aluminum was used as the main material for the model due to its light weight, good machinability, and high surface acoustic impedance. All the aluminum plates except the rear plate were assembled by welding. The rear plate was bolted to the back of the side plates so that it could be disassembled for the installation of interior microphones. It has a $0.5''$ diameter cable hole so that interior microphone cables can be routed through this cable hole. The front and two side plates were firstly assembled to the bottom plate by using aluminum blocks with bolts. The gaps between the plates were filled with welding and excessive welding spots were removed and smoothed by grinding. The similar procedure was also applied for the fillet and top plates.

4.3 Interior Noise Insulation Materials

In order to minimize noise transmitted through the plates, the three layers of the noise insulation materials listed in Table 1 were installed by using spray adhesive inside the plates: the first layer is in contact with the inner surface of the aluminum plates and the last one is inside the interior. The designed noise insulation layers were cut by using a laser cutter at the College of Architecture Woodshop in Texas A&M University.

Table 1: Three layers of interior noise insulation materials.

Layer	Thickness (inch)	Material
1 st layer	1	Polyurethane foam
2 nd layer	0.04	Latex rubber sheet
3 rd layer	0.5	Polyurethane foam

4.4 Windows (Glasses)

The windows were cut from tempered, crystal clear glass with the edges covered with cured silicon by ACME Glass in Bryan, Texas.

4.5 Side Mirror and Rain Gutters

The side mirror was printed from a hard plastic, “Vero White Plus” by rapid prototyping. It was attached on the left side plate with three bolts and used to simulate the aeroacoustic noise generated by a real side mirror.

The rain gutters were needed to reduce the effects of the sharp edges on the aeroacoustic noise. These gutters were printed from a rubber-like soft material, “Tango Black Plus” by using rapid prototyping.

4.6 Supports for Model

The boundary layer thickness in the test section of the KSWT is 0.118 inch [25], the model was mounted at the height of 9.39 inch from the bottom surface of the test section with four supports. The supports were assembled by using hollow pipes and flanges and covered with aluminum sheets in the airfoil shape as shown in Figure 6 to avoid the vortex flow from being generated by the supports.

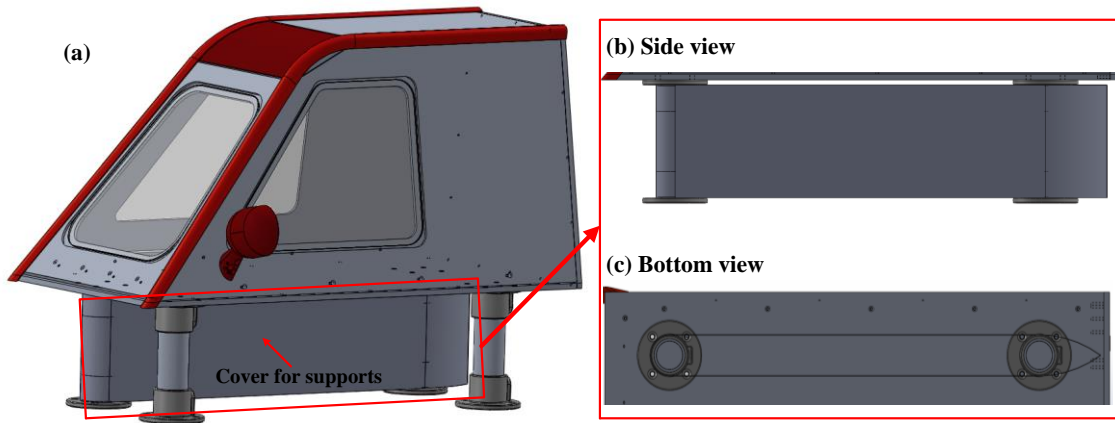


Figure 6: (a) Supports of model and their covers, (b) Side view of cover, and (c) Bottom view of cover.

4.7 Microphone Fairings

1/4" B&K Type 4958 microphones and cables with SMB connectors were used with microphone fairing to measure sound pressure on the surface of the automobile model in the wind tunnel. The microphone fairings were printed by using rapid prototyping to reduce the microphone-induced flow noise, resulting in smooth stream lines around the microphones as shown in Figure 7. Each fairing was designed to have two parts for the easy installation of the microphone. The bottom part was made from a

soft material to absorb the surface vibration transmitted to the microphone, while the top part was made from a hard material. The groove between the microphone and the SMB connector is anchored at the tongue in the top and bottom fairing parts so that the microphone is always installed in the same location inside the fairing.

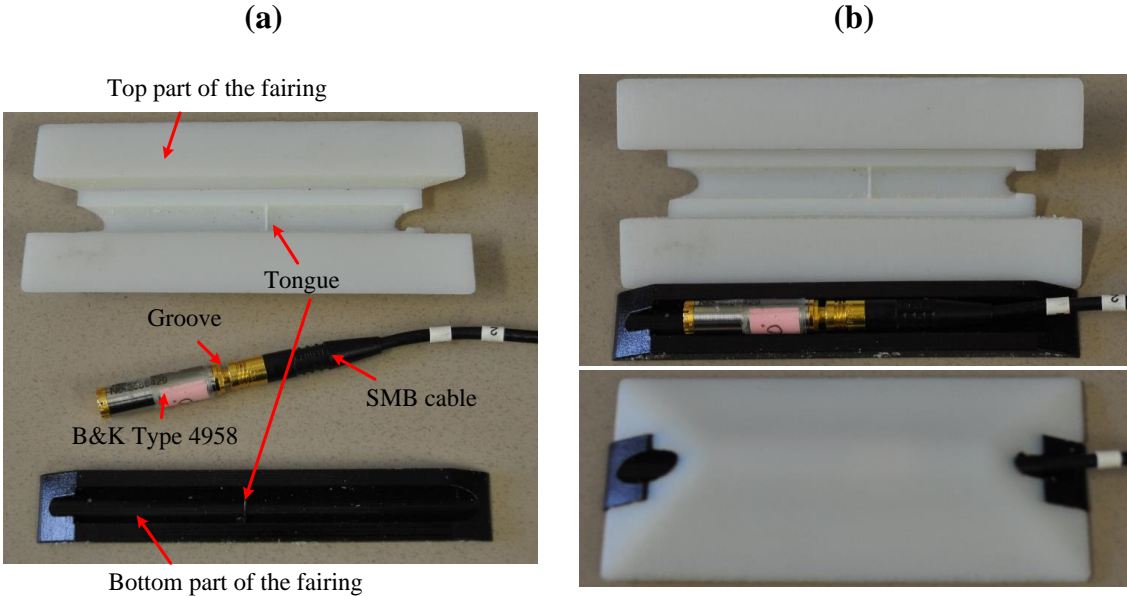


Figure 7: (a) 3-D printed microphone fairing and (b) Assembled with microphone.

5. WIND TUNNEL TEST AND RESULTS*

5.1 Klebanoff-Saric Wind Tunnel

The automobile model was tested at the Klebanoff-Saric Wind Tunnel (KSWT) (see Table 2) that has acoustically treated inner walls so that its background noise level is relatively low. The dimensions of the automobile model were decided by the KSWT test section dimensions. The number of the KSWT fan blades is 9.

Table 2: Information on Klebanoff-Saric Wind Tunnel (KSWT) [26] at Texas A&M University.

Item	Value
Test Section Dimensions (H×W×L)	1.4×1.4×4.9 m (4.5×4.5×16 ft)
Maximum Wind Speed	20 m/s (72 km/h or 44.74 miles/h)
Acoustically Treated Inner Walls	Yes

5.2 Experimental Setup for Wind Tunnel Test

The automobile model was installed in the test section of the KSWT. The bottom flanges of the supports were fixed with bolts to the floor of the test section and the covers of the supports shown in Figure 6 were filled with noise insulation foam and wrapped by using duct tape. Any gaps (or steps) on the surfaces of the automobile

* Parts of this section are reprinted from “Experimental contribution analysis of external aeroacoustic noise components to interior noise of simplified, scaled automobile model in wind tunnel” by Seongil Hwang, Myunghan Lee, Kang Duck Ih, Edward B. White, and Yong-Joe Kim, 2016, *Proceedings of Noise-Con 2016, Providence, RI, United States*, Copyright [2016] with permission by NoiseCon 2016 of INCE-USA.

model, the microphone fairings, and the microphone cables were sealed with vinyl insulation tape to have smooth airflow.

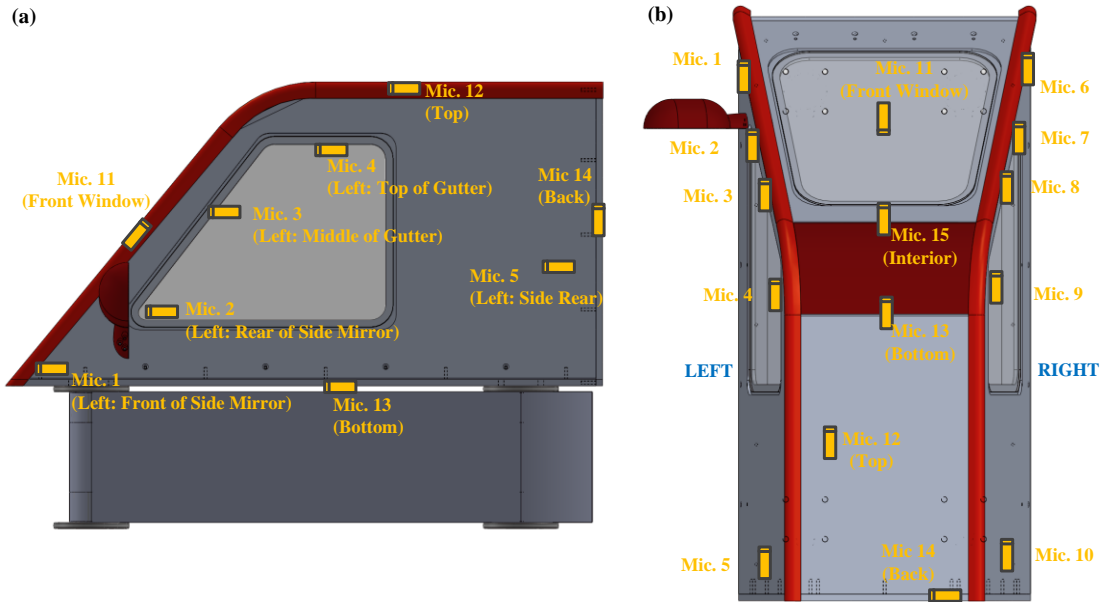


Figure 8: Microphone locations in automobile model: (a) Left side view and (b) Top view.

Table 3: Exterior microphone locations (Refer to Figure 8).

No.	Microphone Position	No.	Microphone Position
1	Left: Front of Side Mirror	8	Right: Middle of Gutter
2	Left: Rear of Side Mirror	9	Right: Top of Gutter
3	Left: Middle of Gutter	10	Right: Rear Side
4	Left: Top of Gutter	11	Front Window
5	Left: Rear Side	12	Top
6	Right: Front of Side Mirror	13	Bottom
7	Right: Rear of Side Mirror	14	Back

For the acoustic pressure measurement, 14 microphones with the fairings were placed on the outer surface of the automobile model and 1 microphone was located inside the model as shown in Figure 8. These 15 B&K Type 4958 microphones were calibrated with the sound calibrator, B&K Sound Calibrator Type 4231 (94 dB @ 1 kHz) in the NI MAX software as in the two speaker experiment. The in-house NI LabVIEW code was again used to acquire the microphone time data at a sampling rate of 20 kHz for 120 seconds.

5.3 Wind Tunnel Test

Table 4: Configurations of wind tunnel test and interior acoustic resonance test.

Airflow Speed	With Interior Noise Treatment	Without Interior Noise Treatment
0 m/s (no flow)	-	Test Configuration 5 (Identification of interior resonances with one speaker and one microphone)
15 m/s	Test Configuration 1	Test Configuration 3
24 m/s	Test Configuration 2	Test Configuration 4

Table 4 shows four wind tunnel test configurations with the two airflow speeds and the two interior noise treatment cases. Firstly, the first two test configurations were conducted at the airflow speeds of 15 m and 24 m/s with the interior noise treatment, and the rest two test configurations were conducted at the same two airflow speeds without any interior noise treatment materials to observe the effects of the noise treatment on the contribution analysis results. In addition to these four test configurations, the interior resonances of the model were measured with one speaker placed inside the model

without any noise treatment materials and driven by a white noise up to 20 kHz. The first blade passing frequency (BPF) of the wind tunnel fan at each flow speed is calculated and shown in Table 5.

The frequency range of the vortex shedding generated by the side mirror can be determined by using the Strouhal Number that includes the information on the flow speed and the dimension of the side mirror. The Strouhal number is approximately 0.2 with the assumption that the model is a cylinder shape [27]. With the consideration of the shortest and longest lengths of the side mirror, the frequency ranges of the vortex shedding at 15 m/s and 24 m/s are from 14.16 Hz to 125.65 Hz and from 22.66 Hz to 201.04 Hz, respectively, as presented in Table 5.

Table 5: Two airflow speeds of KSWT and BPFs of fan at two speeds.

Flow Speed [m/s]	RPM	BPF [Hz]
15	692	103.8
24	1092	163.8

Table 6: Frequency range of vortex shedding caused by side mirror.

Dimension of Side Mirror		Flow Speed	
		15 m/s	24 m/s
Maximum	8.34 inch (0.21184 m)	14.16 Hz	22.66 Hz
Minimum	0.94 inch (0.02388 m)	125.65 Hz	201.04 Hz

5.4 Test Results and Discussion

Figure 9 shows the auto-spectra of the interior microphone and the multiple coherence between the external and internal microphone signals for test configuration 4 at the wind speed of 24 m/s without the interior noise treatment. In the high frequency region above 1 kHz, the multiple coherence is low (e.g., below 0.4), which indicates that the exterior microphones are not capturing entire aeroacoustic noise sources. Thus, the test results from Figure 10 are presented only in the frequency range below 1 kHz.

Figure 10 shows the comparison of the auto-spectra between the four test configurations in Table 4. In Figure 10, the vertical yellow lines indicate the BPF and its harmonics of the wind tunnel fan. With the interior noise treatment installed, the interior noise level is approximately 70 dB lower than the exterior noise levels around 1 kHz. Even when the noise treatment materials are removed, the interior noise level is still approximately 40 dB lower than the exterior noise levels around 1 kHz. This large noise reduction even without the interior noise treatment is caused by the 7/16-inch-thick aluminum panels. They can cause the high sound transmission loss, significantly reducing the transmitted noise from the exterior to the interior, in particular, at high frequencies. In addition, the 24 m/s airflow cases show higher noise levels than the 15 m/s cases, thus having higher signal-to-noise ratio (SNR) than the 15 m/s cases. Therefore, the only results for test configuration 4 at the airflow speed of 24 m/s without the interior noise treatment, are presented below, in which the contribution of the exterior aeroacoustic noise sources to the interior noise is more distinctly presented than other test configurations due to the high SNR.

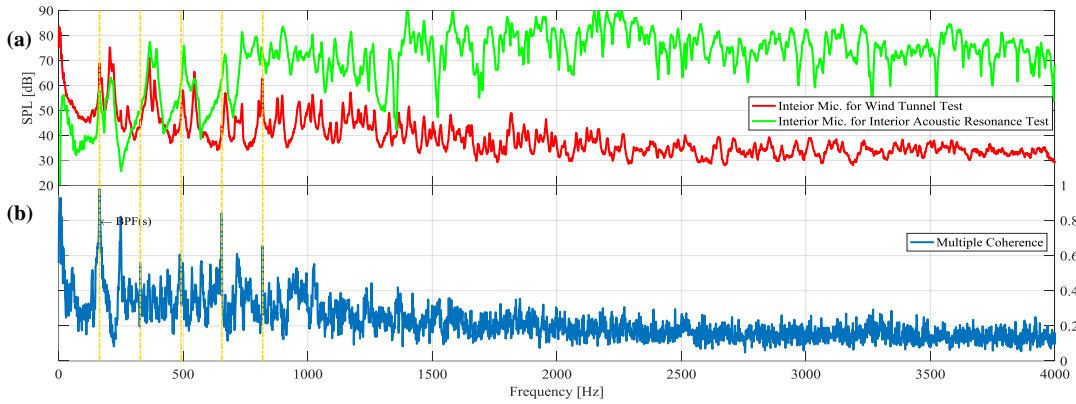


Figure 9: Wind tunnel test results at airflow speed of 24 m/s without interior noise treatment in frequency range up to 4 kHz. (a) Auto-spectrum of interior microphone in both wind tunnel test and interior acoustic resonance test and (b) Multiple coherence between exterior and interior microphone signals in wind tunnel test.

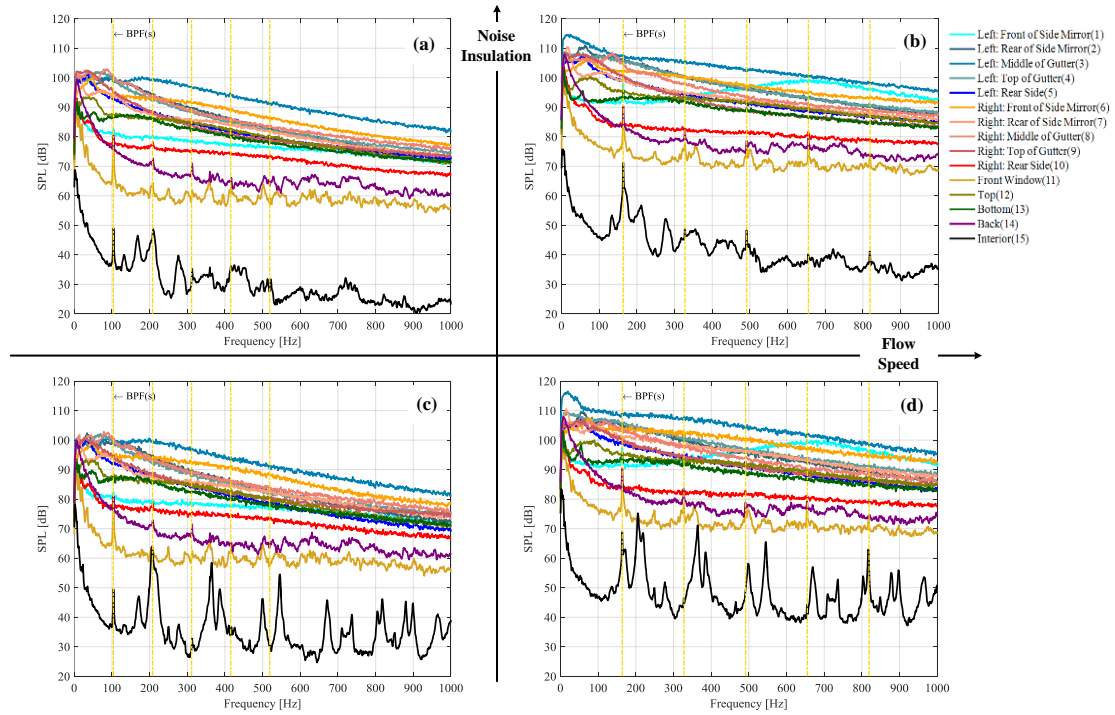


Figure 10: Comparison of auto-spectra measured by using exterior and interior microphones in 4 test configurations. (a) 15 m/s with interior noise treatment, (b) 24 m/s with interior noise treatment, (c) 15 m/s without interior noise treatment, and (d) 24 m/s without interior noise treatment.

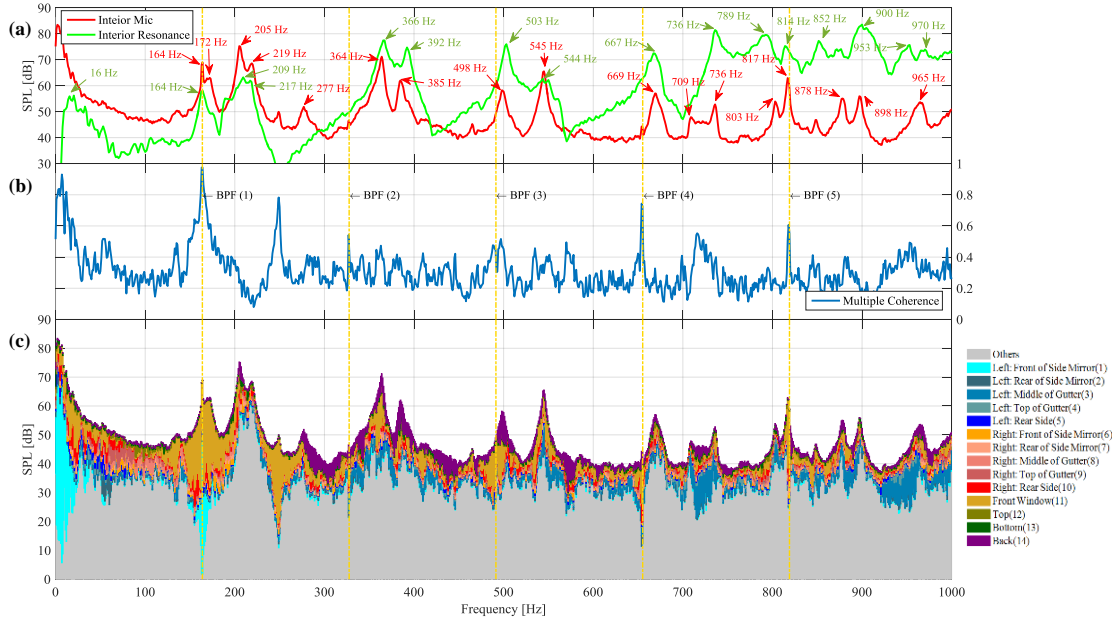


Figure 11: Results of wind tunnel test at flow speed of 24 m/s without interior noise treatment and interior resonance test without both airflow and interior noise treatment. (a) Auto-spectrum of interior microphone, (b) Multiple coherence between exterior and interior microphone signals, and (c) Interior auto-spectrum decomposed by using normalized contribution.

Figure 11 shows the contribution analysis results along with the interior auto-spectra and the multiple coherence up to 1k Hz for test configuration 4. Figure 12 and Figure 13 show the zoomed views of Figure 11 at selected interior noise peak frequencies and Table 7 and Table 8 presents the first three highest contributions of the exterior noise sources to the interior noise at the selected frequencies. Table 3 presents the exterior microphone numbers and their locations used in Table 7 and Table 8.

The frequency of 164 Hz (Figure 12(a)) coincides with the BPF, the one of the interior resonance frequencies, and the vortex shedding frequency caused by the side mirror (see Table 6). As shown in Table 7 and Table 8, the first two highest

contributions are from the front of the left side mirror and the left rear side at the normalized contributions of 35.92 % and 23.01 %, respectively, indicating that the vortex shedding generated from the left side mirror is dominantly contributing to the interior noise at 164 Hz. Most of the selected interior noise peaks (e.g., 205 Hz, 669 Hz, 803 Hz, 878 Hz, and 965 Hz) in Figure 12 and Figure 13 are mainly generated from the interior resonances. Thus, the multiple coherence is low at these interior resonance frequencies. At these frequencies, unless there are other causes to generate the interior noise peaks, all the aeroacoustic sources contribute insignificantly with the maximum single source contribution of approximately 15 % or below. Although the peak at 364 Hz (Figure 12(c)) seems to be generated by the interior resonance, the multiple coherence is approximately 0.5 indicates that the vortex shedding at the back (13.04 %) and the airflow on the front window (10.99 %) are also contributing meaningfully to the interior noise. The peaks at 498 Hz (Figure 12(d)) and 736 Hz (Figure 13(a)) are also generated by the interior resonances, although the aeroacoustic noise sources at the front window, the left gutter, and the back are largely contributing to the interior noise. The 5th harmonics of the BPF is almost coincident with the interior noise peak at 817 Hz, indicating that the noise generated by the wind tunnel fan is dominant. At this frequency, the front window has the highest contributions of 34.25 % as shown in Table 8.

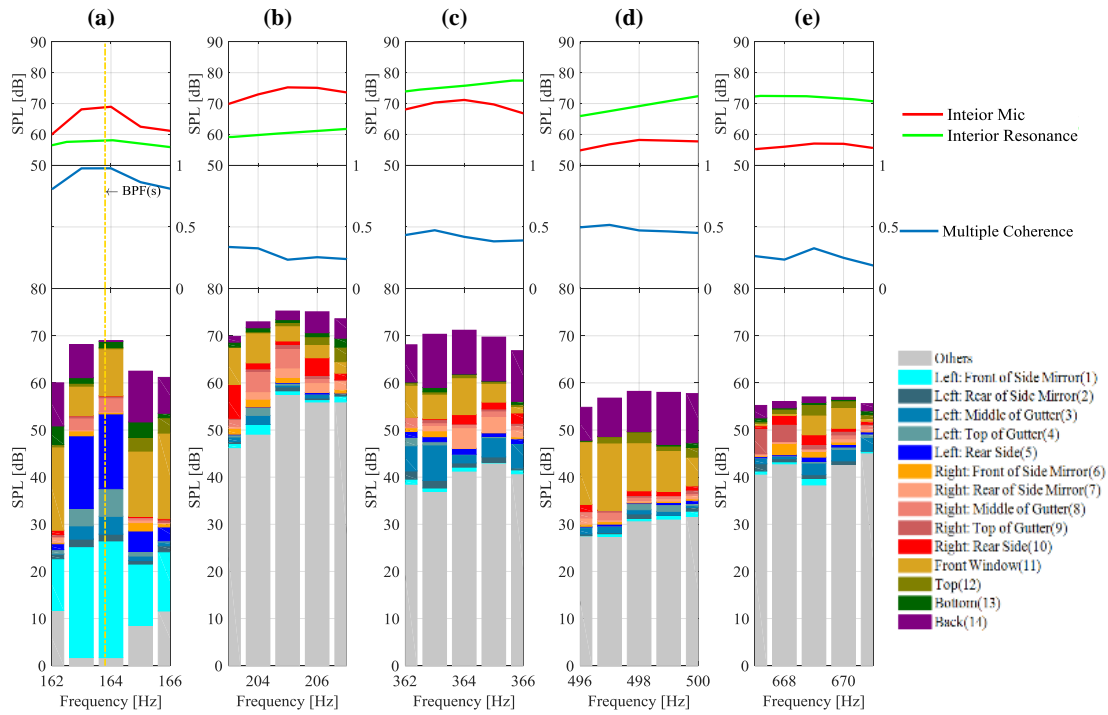


Figure 12: Zoomed contribution results: (a) 164 Hz, (b) 205 Hz, (c) 364 Hz, (d) 498 Hz, and (e) 669 Hz.

Table 7: First three highest contributions at selected interior noise peak frequencies in Figure 12.

Frequency [Hz]		164	205	364	498	669
1st	Microphone No.	1	8	14	11	11
	Contribution [%]	35.92	5.5	13.04	17.53	7.34
2nd	Microphone No.	5	11	11	14	3
	Contribution [%]	23.01	4.29	10.99	14.67	4.33
3rd	Microphone No.	11	7	7	12	12
	Contribution [%]	14.5	2.59	6.14	4.01	3.97

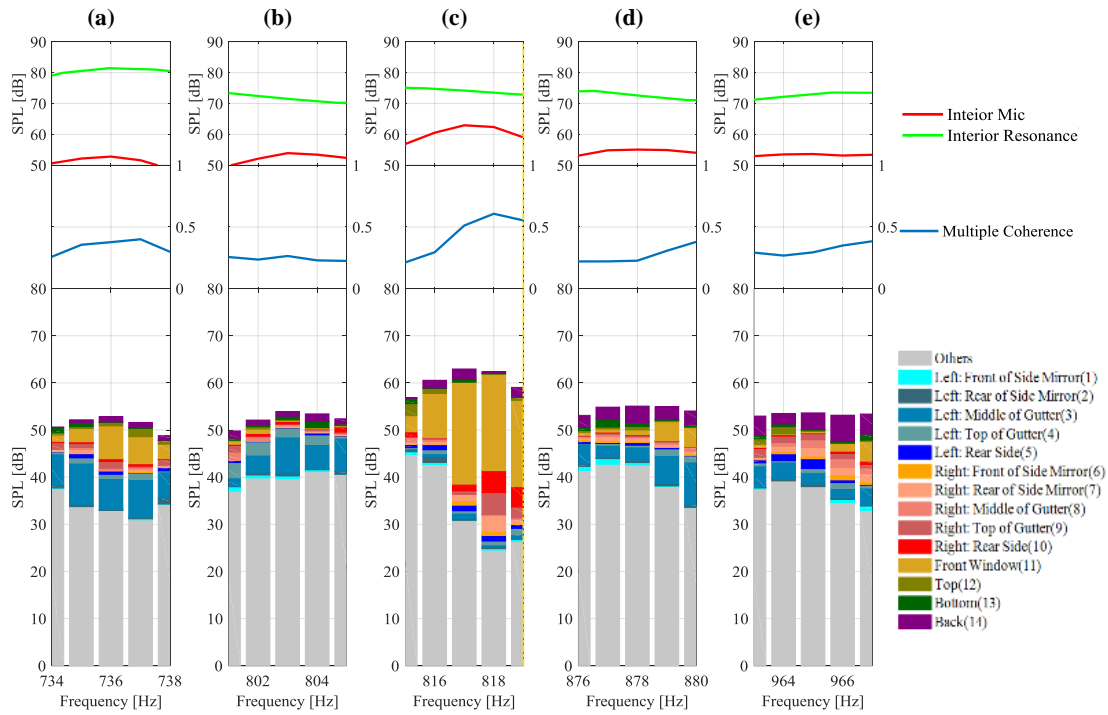


Figure 13: Zoomed contribution results: (a) 736 Hz, (b) 803 Hz, (c) 817 Hz, (d) 878 Hz, and (e) 965 Hz.

Table 8: First three highest contributions at selected interior noise peak frequencies in Figure 13.

Frequency [Hz]		736	803	817	878	965
1st	Microphone No.	11	3	11	14	14
	Contribution [%]	13.17	14.5	34.25	6.18	6.55
2nd	Microphone No.	5	11	11	14	3
	Contribution [%]	12.59	3.62	3.51	5.34	4.52
3rd	Microphone No.	11	7	7	12	12
	Contribution [%]	2.77	1.86	2.27	1.84	3.88

6. EXPERIMENT WITH AUTOMOBILE AND RESULTS

6.1 Experimental Setup for Automobile Test

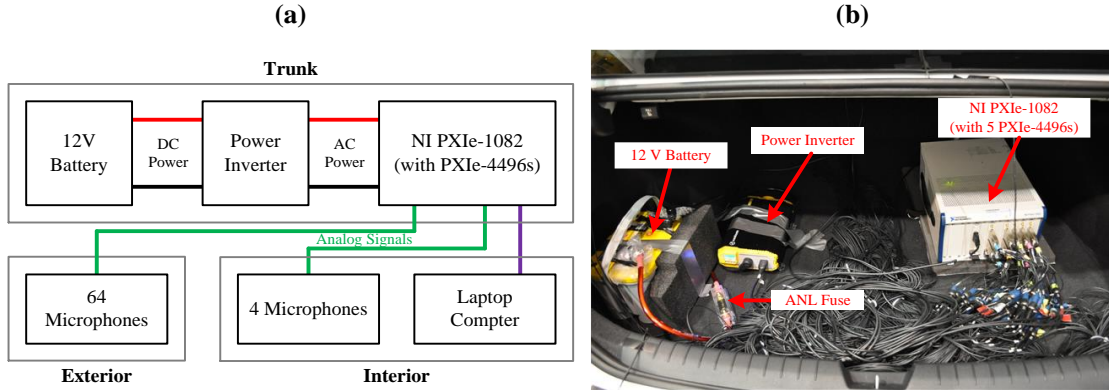


Figure 14: Experimental setup with automobile: (a) Schematic of equipment connection and (b) Equipment inside automobile's trunk.

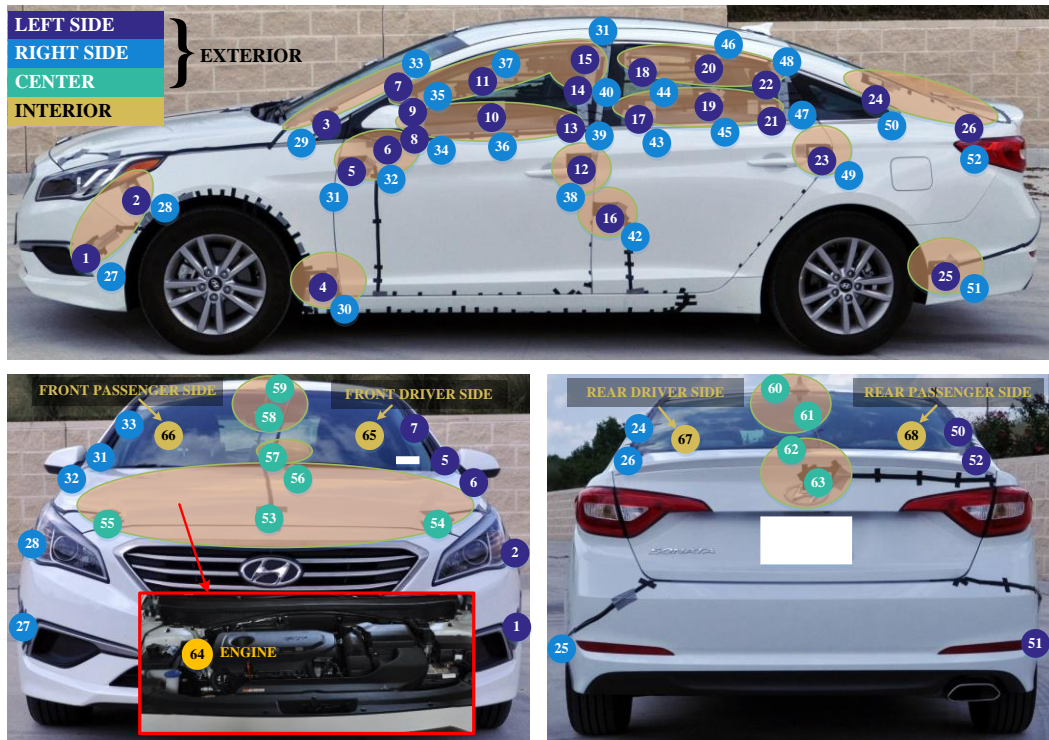


Figure 15: Microphone installation locations. Refer to Table 9 for the description of the microphone locations.

An automobile (Hyundai Sonata) was instrumented and tested on a road at the two cruising speeds of 65 mph and 80 mph. Figure 14(a) shows the schematic diagram of the instrumentation for this experiment. A 12V battery and a power inverter were used to power a NI PXIe-1082 chassis with five NI PXIe-4496 data acquisition modules. The measurement equipment was placed in the trunk shown in Figure 14(b) to avoid the fan noise, of the NI PXIe-1082 chassis, that contaminated interior microphone signals. The in-house NI LabVIEW code from the previous two speaker experiment was reused to acquire the time data of both 64 exterior and 4 interior microphones at a sampling rate of 20 kHz for 30 seconds.

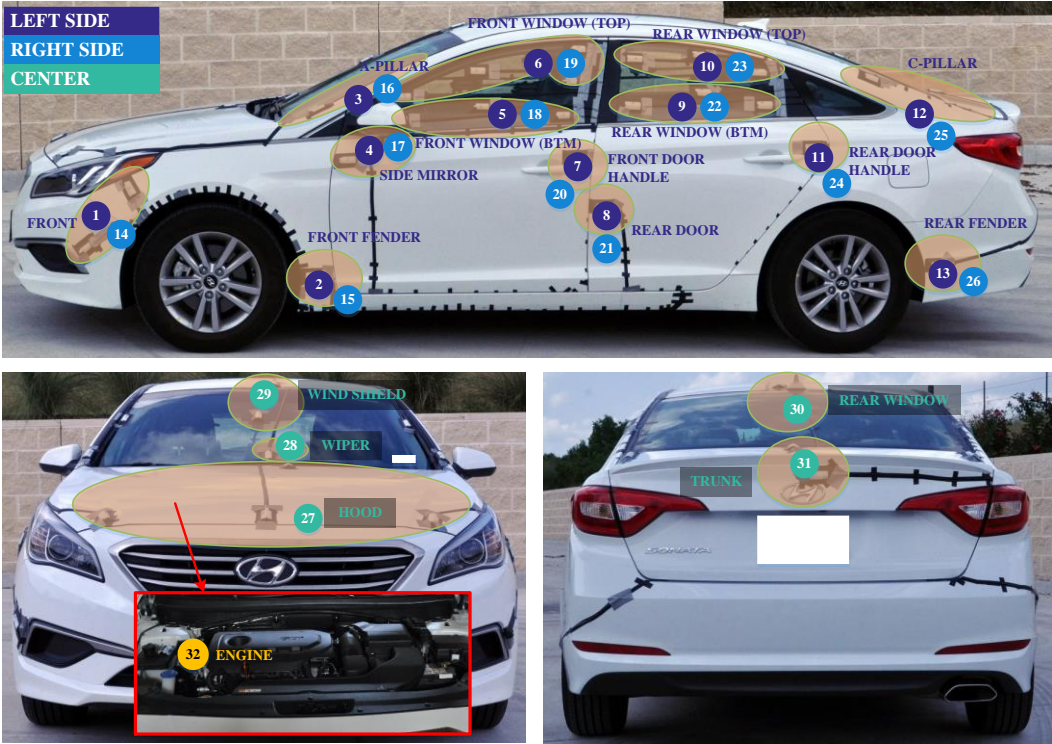


Figure 16: Locations of grouped microphones. Refer to Table 10 for the description of the microphone groups.

Table 9: List of noise source microphone locations (Refer to Figure 15).

No.	Position	No.	Position
1	Left of front bumper	33	Right wind shield
2	Bottom of left headlamp	34	Lower front of front right window
3	Front of left A-pillar	35	Upper front of front right window
4	Rear of front left fender	36	Lower middle of front right window
5	Front of left side mirror	37	Upper middle of front right window
6	Bottom of left side mirror	38	Front of right door handle
7	Left wind shield	39	Lower rear of front right window
8	Lower front of front left window	40	Middle rear of front right window
9	Upper front of front left window	41	Upper rear of front right window
10	Lower middle of front left window	42	Middle front of rear right door
11	Upper middle of front left window	43	Lower front of rear right window
12	Front of left door handle	44	Upper front of rear right window
13	Lower rear of front left window	45	Lower middle of rear right window
14	Middle rear of front left window	46	Upper middle of rear right window
15	Upper rear of front left window	47	Lower rear of rear right window
16	Middle front of rear left door	48	Upper rear of rear right window
17	Lower front of rear left window	49	Rear of right door handle
18	Upper front of rear left window	50	Right C-pillar
19	Lower middle of rear left window	51	Rear of rear right fender
20	Upper middle of rear left window	52	Right of trunk door
21	Lower rear of rear left window	53	Front middle hood
22	Upper rear of rear left window	54	Front left hood
23	Rear of left door handle	55	Front right hood
24	Left C-pillar	56	Rear middle hood
25	Rear of rear left fender	57	Front middle wind shield
26	Left of trunk door	58	Middle of wind shield
27	Right of front bumper	59	Front middle ceiling
28	Bottom of right headlamp	60	Rear middle ceiling
29	Front of right A-pillar	61	Middle of rear window
30	Rear of front right fender	62	Upper middle of trunk door
31	Front of right side mirror	63	Rear middle of trunk door
32	Bottom of right side mirror	64	Engine

Table 10: Grouping of noise source microphones (Refer to Figure 16).

No.	Group Name	Mic. No.
1	Left of front bumper	1, 2
2	Rear of front left fender	4
3	Left A-pillar	3, 7
4	Left side mirror	5, 6
5	Lower area of front left window	8, 10, 13
6	Upper area of front left window	9, 11, 14, 15
7	Front left door handle	12
8	Rear left door	16
9	Lower area of rear left window	17, 19, 21
10	Upper area of rear left window	18, 20, 22
11	Rear left door handle	23
12	Left C-pillar	24, 26
13	Rear of rear left fender	25
14	Right of front bumper	27, 28
15	Rear of front right fender	30
16	Right A-pillar	29, 33
17	Right side mirror	31, 32
18	Lower area of front right window	34, 35, 36
19	Upper area of front right window	37, 39, 40, 41
20	Front right door handle	38
21	Rear right door	42
22	Lower area of rear right window	43, 44, 45
23	Upper area of rear right window	46, 47, 48
24	Rear right door handle	49
25	Right C-pillar	50, 52
26	Rear of rear right fender	51
27	Hood	53, 54, 55, 56
28	Wiper	57
29	Wind shield	58, 59
30	Rear window	60, 61
31	Trunk door	62, 63
32	Engine	64

Sixty-three 1/4" B&K Type 4958 microphones along with microphone fairings (see Figure 7) were installed on the outer surface of the automobile to measure external

aeroacoustic noise signals. Here, the microphone fairings were used to reduce the microphone-induced flow noise, resulting in smooth stream lines around the microphone and fairing assemblies. One 1/4" B&K Type 4958 microphone was also located close to the engine in the engine room to acquire the engine noise data. Exterior microphone cables were covered by using plastic insulation tapes to reduce the cable-induced flow noise. Four 1/2" B&K Type 4189-A-021 microphones were placed on the window-side head rests at the four seat positions to measure the interior noise signals. Figure 15 and Table 9 show the channel numbers of all the microphones and their locations. As shown in Figure 15, 26 microphones were installed at each side of the automobile, 11 microphones on the other exterior surfaces except the underbody of the automobile, and 1 microphone inside the engine room. Figure 16 and Table 10 show 32 microphone groups to effectively observe the contributions of the areas covered by the grouped microphones to the interior noise.

6.2 Test Results and Discussion

Figure 17 shows the 1/3 octave band contributions, in dBA, of the microphone groups to the interior noise at the front driver side seat and the automobile speed of 80 mph. At first glance, it can be observed that the contribution of the front left window (groups 5 and 6) closed to the front driver side seat seems to be high compared to other groups, although it is difficult to be quantitatively compared to the other contributions. Therefore, the overall contributions of all the microphone groups were presented in Figure 18. The first nine highest contributions were observed at the four windows and the hood: i.e., from the highest to the lowest, the upper area of the front left window

(group 6), the upper area of the front right window (group 19), the lower area of the front left window (group 5), the hood (group 27), the lower area of the front right window (group 18), the lower area of the rear right window (group 22), the upper area of the rear right window (group 23), the upper area of the rear left window (group 10), and the lower area of the rear left window (group 9). The contribution of the engine to the interior noise (group 32) was ranked at 22th in this case, indicating that the engine noise is not significantly contributing to the interior noise during the cruise condition at 80 mph.

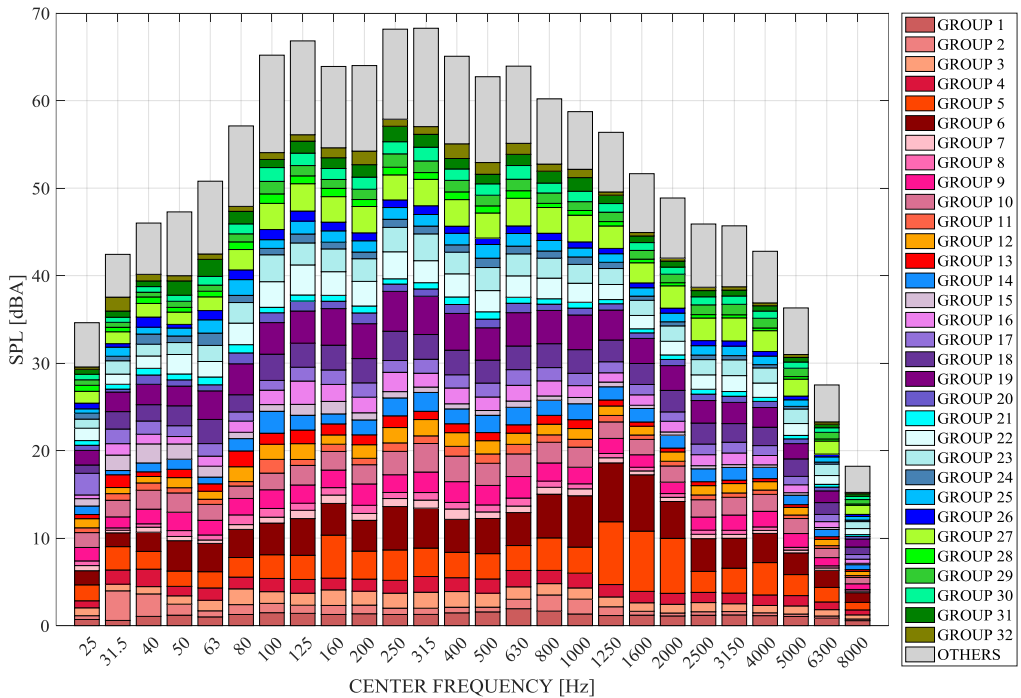


Figure 17: 1/3 octave band contributions of microphone groups (Figure 16 and Table 10) to interior noise at front driver side seat in dBA at automobile speed of 80 mph..

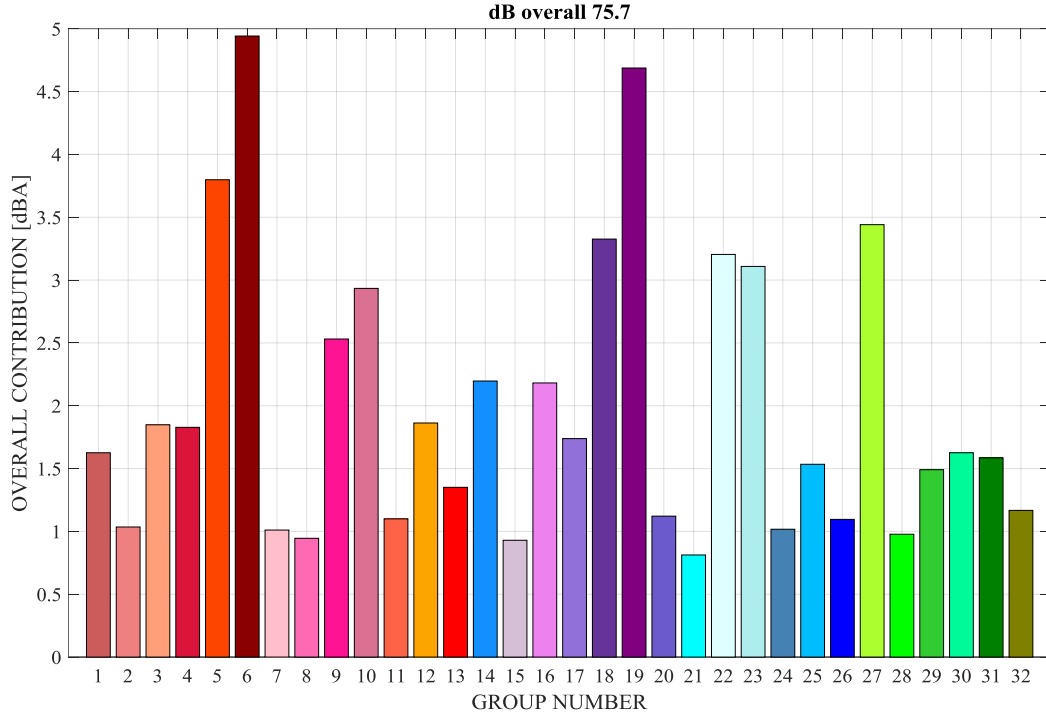


Figure 18: Overall contribution results of microphone groups (Figure 16 and Table 10) to interior noise at front driver side seat at speed of 80 mph.

Figure 19 and Figure 20 show the effects of the automobile speed and the interior microphone position, respectively, on the contributions. In Figure 19, the two data sets at the speeds of 65 mph and 80 mph with the receiver microphone at the front driver side seat were used to analyze the effects of the automobile’s cruising speed on the contributions. As shown in Figure 19, the highlighted contributions of the three windows (groups 5, 6, 19, and 22), the left C-pillar (group 12), the rear area of rear right fender (group 13), the right side of the front bumper (group 14), and the right A-pillar (group 16), were increased when the automobile speed was increased. The highest contribution difference of 0.557 dBA between the two speeds was observed at the front

left window (group 6) that was close to the measured seat position. This difference may be caused mainly by the vortices generated by both the left side mirror and the A-pillar.

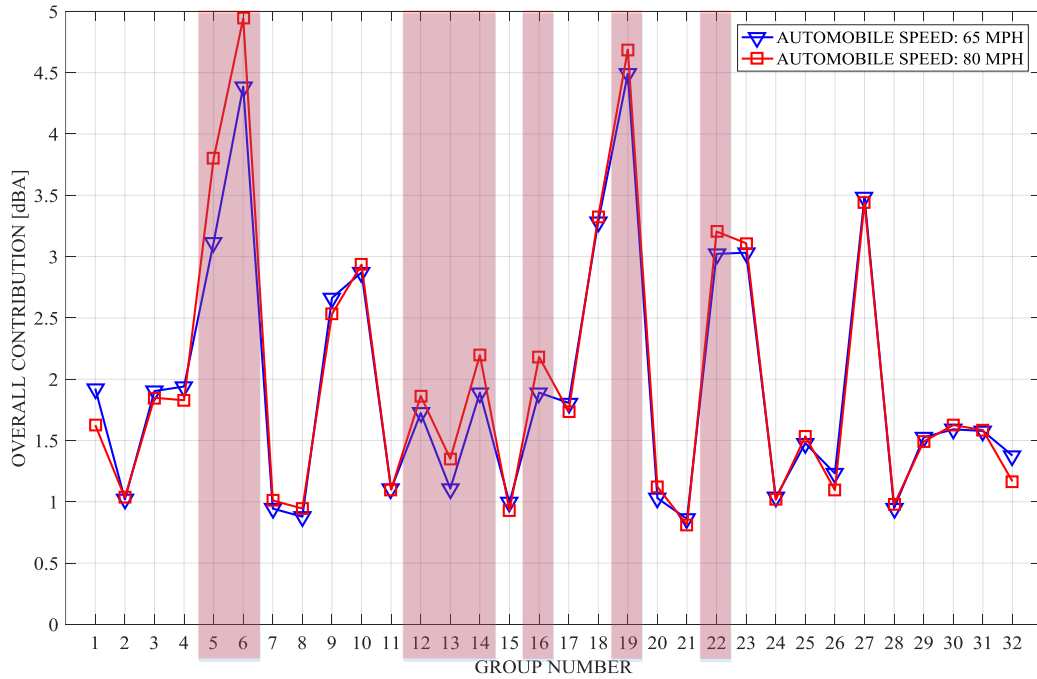


Figure 19: Effects of automobile speeds on overall contribution of microphone groups (Figure 16 and Table 10) at front driver side seat.

Regarding the effects of the seat position on the contributions, one data set with the four interior microphone signals at the speed of 80 mph was analyzed as shown in Figure 20. Here, the contribution differences between the seat positions in most microphone groups were small except the microphone groups at the four windows. The contributions of the four window areas were highlighted with different colors. In microphone groups 5 and 6 at the front left window, the highest contribution was observed at the front driver side seat, which is close to the front left window. Similarly,

microphone groups 18 and 19 at the front right window, close to the front passenger side seat, had the highest contribution, and the contributions of microphone groups 22 and 23 (the rear right window) at the rear passenger side seat was the highest. In summary, the high contribution at a specific seat could be obtained from the window area close to the seat.

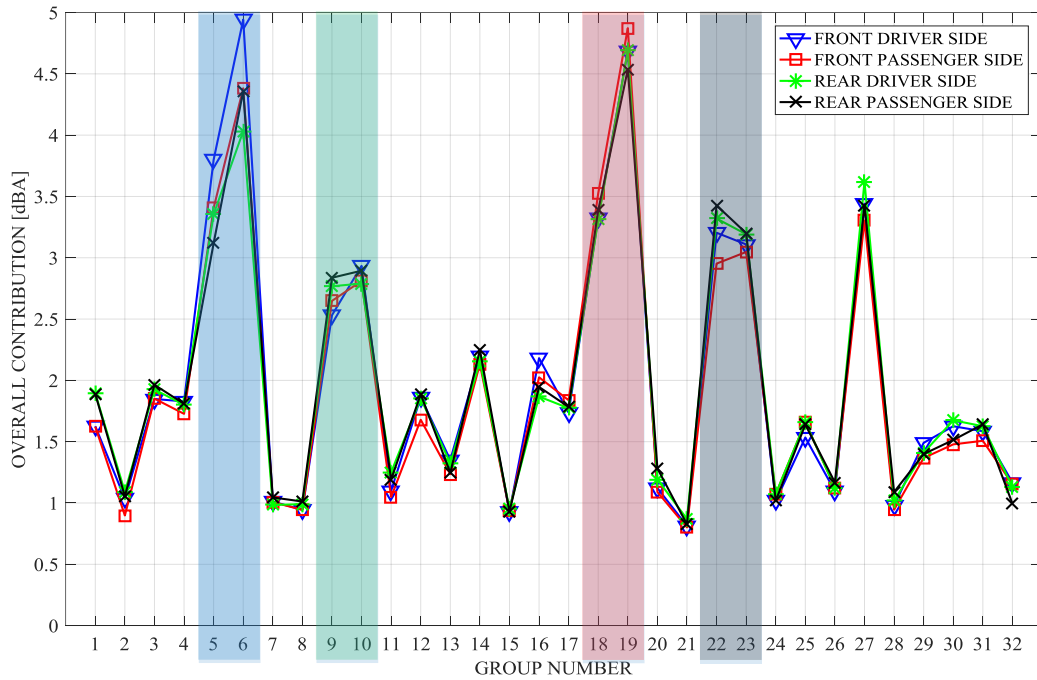


Figure 20: Effects of seat positions on overall contribution of microphone groups (Figure 16 and Table 10) at automobile speed of 80 mph.

7. MICROPHONE-ARRAY-MEASUREMENT-BASED CONTRIBUTION ANALYSIS

In order to analyze the contributions of exterior aeroacoustic noise sources in an automobile using the proposed CD-based procedure, it is required to install microphones flush-mounted on the exterior surface of the automobile to measure the noise source signals. However, the surface-flush-mounted microphone installation can be labor-intensive and time-consuming, making it difficult to evaluate a large number of aeroacoustic design cases.

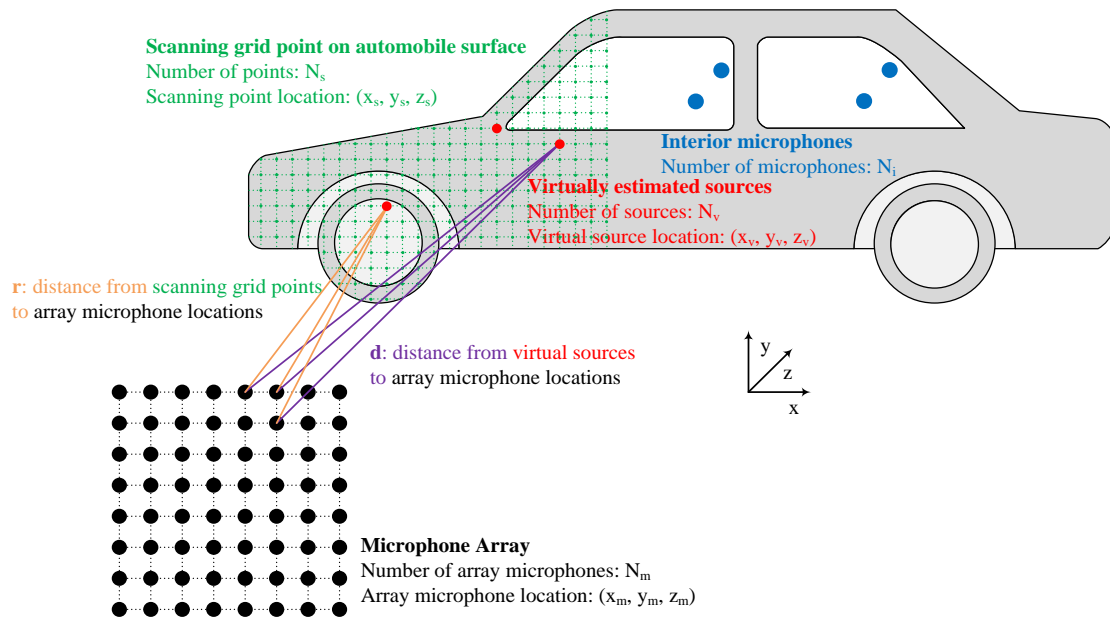


Figure 21: Scheme of beamforming based contribution analysis.

7.1 Identification of Source Locations Using Two Beamforming Methods

When N_m array microphones are used to measure acoustic pressure signals as shown in Figure 21, the vector of the measured acoustic pressure signals, \mathbf{p}_m can be represented at a single frequency of f as

$$\mathbf{p}_m(f) = [p_1(f) \ \cdots \ p_{N_m}(f)]^T. \quad (10)$$

The N_m by N_m cross-spectral matrix (CSM), \mathbf{S}_{mm} can then be built by using the measured array microphone signals as

$$\mathbf{S}_{mm}(f) = \mathbb{E}\{\mathbf{p}_m(f)\mathbf{p}_m^H(f)\} = \begin{bmatrix} \mathbf{S}_{11}(f) & \cdots & \mathbf{S}_{1N_m}(f) \\ \vdots & \ddots & \vdots \\ \mathbf{S}_{N_m1}(f) & \cdots & \mathbf{S}_{N_mN_m}(f) \end{bmatrix}. \quad (11)$$

The N_m by N_s steering vector, \mathbf{W} between the array microphones and the 2-D scanning points, with the assumption of the monopole sound radiation from the scanning points to the microphones, can be represented as

$$\mathbf{W} = \begin{bmatrix} \frac{1}{r_{11}} e^{ikr_{11}} & \cdots & \frac{1}{r_{1N_s}} e^{ikr_{1N_s}} \\ r_{11} & & r_{1N_s} \\ \vdots & \ddots & \vdots \\ \frac{1}{r_{N_m1}} e^{ikr_{N_m1}} & \cdots & \frac{1}{r_{N_mN_s}} e^{ikr_{N_mN_s}} \\ r_{N_m1} & & r_{N_mN_s} \end{bmatrix}, \quad (12)$$

where N_s is the number of the scanning points, r is the distance from the scanning point (x_s, y_s, z_s) to the microphone location (x_m, y_m, z_m) , and k is the wave number.

The Delay And Sum (DAS) and Multiple Signal Classification (MUSIC) beamforming powers can then be expressed as Eq. (13) and Eq. (14), respectively:

$$\mathbf{B}_{\text{DAS}} = \mathbf{W}^H \mathbf{S}_{mm} \mathbf{W} \quad (13)$$

$$\mathbf{B}_{\text{MUSIC}} = \frac{1}{\sum_{i=nd+1}^M |\mathbf{W}^H \cdot \mathbf{u}_i|^2}, \quad (14)$$

where \mathbf{u}_i is the i -th column vector of the factorized unitary matrix \mathbf{U} obtained by applying the SVD to \mathbf{S}_{mm} (i.e., $\mathbf{S}_{mm} = \mathbf{U} \cdot \mathbf{\Sigma} \cdot \mathbf{V}^H$) and nd is the dimension of the signal space. The virtual source locations can then be determined at the locations of the local beamforming power maxima.

7.2 Reconstruction of Virtual Source Signals from Measured Array Signals

When the sound radiation characteristics from noise sources to the array microphones are same as the monopoles, the acoustic pressure vector, \mathbf{p}_m measured by using the array can be represented with the N_m by N_v propagator matrix, \mathbf{G} between the virtual source locations and the array microphone locations as

$$\mathbf{p}_m = \mathbf{G}\mathbf{v}, \quad (15)$$

where \mathbf{v} is the complex amplitude vector of the virtual sources and the propagator matrix \mathbf{G} is defined as

$$\mathbf{G} = \begin{bmatrix} \frac{1}{d_{11}} e^{ikd_{11}} & \dots & \frac{1}{d_{1N_v}} e^{ikd_{1N_v}} \\ \vdots & \ddots & \vdots \\ \frac{1}{d_{N_m1}} e^{ikd_{N_m1}} & \dots & \frac{1}{d_{N_mN_v}} e^{ikd_{N_mN_v}} \end{bmatrix}, \quad (16)$$

where N_v is the number of the virtual sources, d is the distance from the virtual source (x_v, y_v, z_v) to the microphone location (x_m, y_m, \mathbf{z}_m) .

By substituting Eq. (15) into Eq. (11), Eq. (11) can be rewritten as

$$\mathbf{S}_{mm} = \mathbf{E}(\mathbf{G}\mathbf{v}\mathbf{v}^H\mathbf{G}^H) = \mathbf{G}\mathbf{S}_{vv}\mathbf{G}^H, \quad (17)$$

where \mathbf{S}_{vv} is the CSM of the virtual sources defined as

$$\mathbf{S}_{vv} = \mathbf{E}(\mathbf{v}\mathbf{v}^H). \quad (18)$$

Then, the CSM of the virtual sources can be determined from Eq. (18) as

$$\mathbf{S}_{vv} = (\mathbf{G}^H\mathbf{G})^{-1} \mathbf{G}^H\mathbf{S}_{mm}\mathbf{G}(\mathbf{G}^H\mathbf{G})^{-1}. \quad (19)$$

Similarly, the CSM between the virtual sources and the interior microphone signals can be represented as

$$\mathbf{S}_{vi} = (\mathbf{G}^H\mathbf{G})^{-1} \mathbf{G}^H\mathbf{S}_{mi}, \quad (20)$$

where \mathbf{S}_{mi} is the CSM between the array microphone signals and the interior noise signals. Then, the CD-based contribution analysis can be applied to \mathbf{S}_{vv} and \mathbf{S}_{vi} , resulting in the contributions of the virtual sources to the interior noise.

7.3 Experimental Setup for Validation

For the validation of beamforming based contribution, experimental data was acquired with the configuration as shown in Figure 22. 3 speakers were located with distances 0.6 m and 0.4 m, respectively. The speakers were driven by three independent, filtered white noise signals using NI PXI-4461 for two speakers and B&K PULSE 3560-B-130 for one speaker. The excited signals as shown in Figure 22(a) were low-pass filtered white noise up to 2.2 kHz for speaker 1, band pass filtered white noise from 1.7 kHz to 3.3 kHz for speaker 2, and band pass filtered white noise from 2.8 to 5.5 kHz. 9 B&K Type 4189-A-021 (1/2") microphones were used as reference microphones for the

reference contribution analysis, and located the upper unit of a speaker, the lower unit of a speaker, and the middle point of the both units per each speaker.

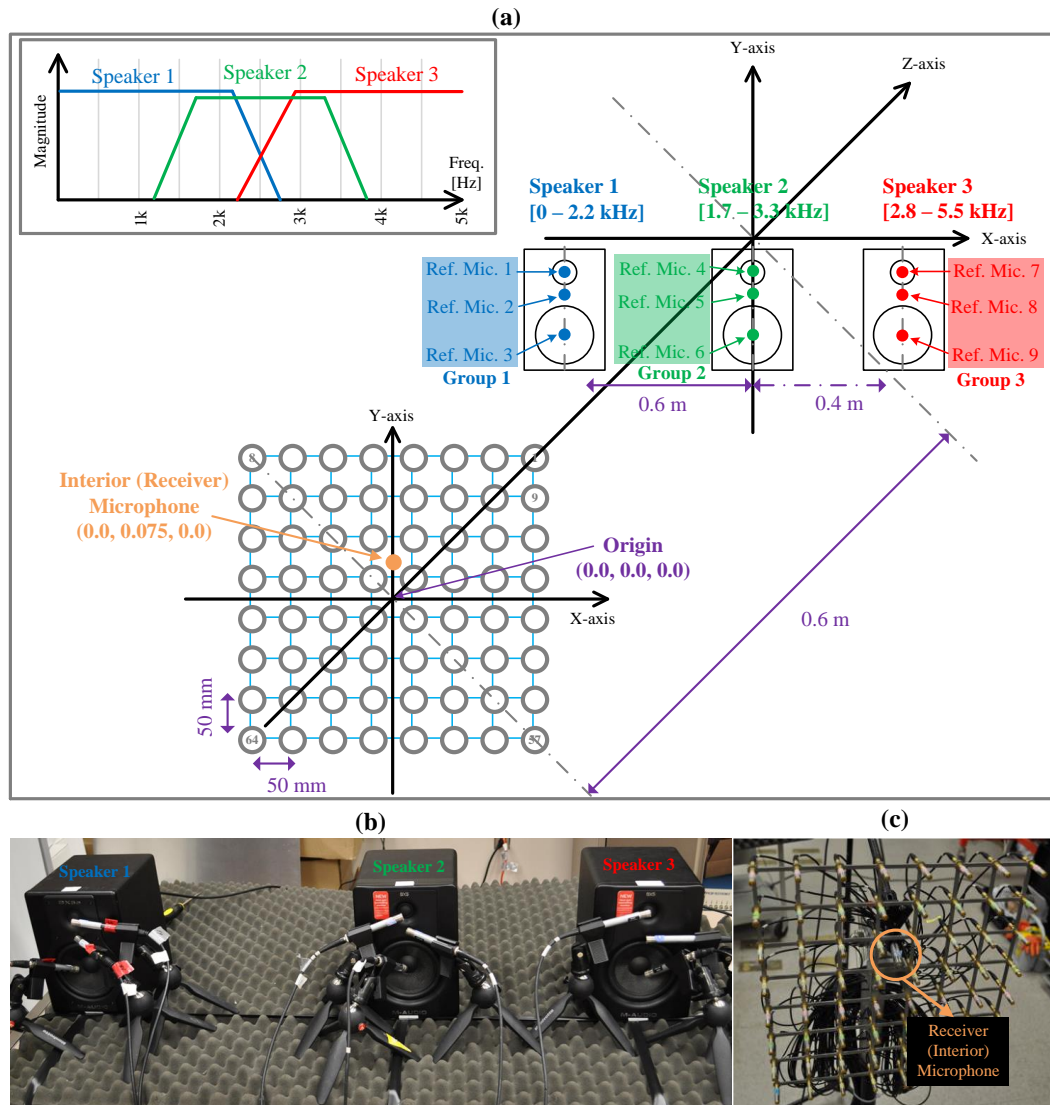


Figure 22: Experimental setup for validation of beamforming with microphone array and CD-based contribution analysis procedure: (a) Illustration of experimental setup, (b) Three speakers with the nine reference microphones, and (c) the microphone array and receiver microphone placed at the center of the array.

The microphone array was consisting of 64 B&K Type 4958 (1/4”) microphones in a square shape with the 0.05 m, 0.05 m spacing of x-axis and y-axis, respectively. The microphone array was located 0.6 m from the speakers in z-axis, and the receiver microphone was located in the middle of the microphone array. The one receiver microphone of B&K Type 4189-A-021 (1/2”) was located the center of the microphone array. NI PXIe-1082 with five NI PXIe-4496 and in-house NI LabVIEW were used to acquire signals for 60 seconds.

7.4 Test Results and Discussions

Figure 23 and Figure 24 show the DAS and MUSIC beamforming powers reconstructed on the front surface of speakers by using the measured array data. In Figure 23 and Figure 24, the local beamforming maximum locations are coincident with the locations of the locations of the speaker driver unit(s) depending on the reconstruction frequencies, indicating that the local beamforming power locations can be correctly identified as noise source locations. Then, the noise source signals to calculate the contributions of the noise sources are reconstructed from the measured array signals at the local beamforming power locations. The noise source signals reconstructed from the measured array signals are referred to as “virtual” source signals, while the ones measured by using the real reference microphones, as “real” source signals. In this source reconstruction process, the noise propagation characteristics from a virtual source location to the array microphone locations are assumed to be the same as those of a monopole. That is, all the virtual sources are assumed to be monopoles.

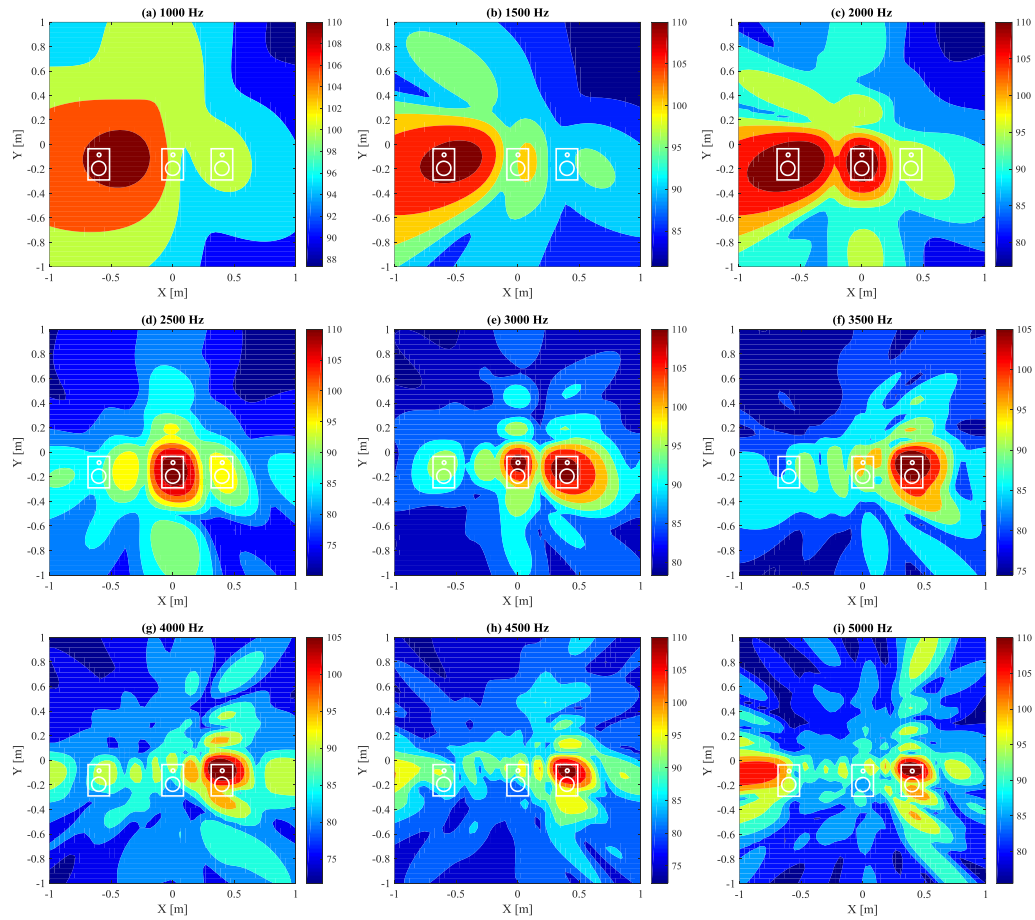


Figure 23: DAS beamforming powers on the front of the three speakers at different frequencies: (a) 1 kHz, (b) 1.5 kHz, (c) 2 kHz, (d) 2.5 kHz, (e) 3 kHz, (f) 3.5 kHz, (g) 4 kHz, (h) 4.5 kHz, and (i) 5 kHz. Notes that white lines in the plot show the locations of the speakers, and speaker units.

Figure 25 shows the contributions of the “real” source signals and the “virtual” source signals. Here, the real source signals were measured by using the real reference microphones placed close to the three speakers. In addition, the source signals measured by using the three reference microphones placed in front of each speaker were grouped as a single group: i.e., group 1 for the three reference microphone signals measured in front of speaker 1, group 2 for speaker 2, and group 3 for speaker 3 (See Figure 22(a)).

The three virtual source signals were reconstructed from the array microphone signals at the maximum beamforming locations of 1.5 kHz (Figure 23(b) and Figure 24(b)), 2.5 kHz (Figure 23(d) and Figure 24(d)), and 3.5 kHz (Figure 23(f) and Figure 24(f)). The maximum contribution (i.e., the total of all the three contributions) in percent indicate how much real or virtual source signals are correlated with the interior microphone signal measured at the center of the array. The total contributions of the virtual source signals are mostly higher than those of the real source signals, indicating that the effects of background noise on the contributions of the real source signals are higher than those of the virtual source signals since the virtual source locations can be closer to the speakers than the real microphone locations. Due to the same reason, the contributions of the virtual source signals in low, mid, and high frequency regions can be separated better than those of the real signal groups. For example, speaker 1 generated low frequency noise (e.g., below 1.7 kHz) dominantly. Thus, the contributions of real signal group 1 and virtual source 1 are dominant in this frequency region. When comparing Figure 25(a) and Figure 25(b) in the low frequency region, the contributions of virtual source 1 is higher than those of real signal group 1 since the real reference microphones close to speaker 1 can measure more noise generated from the two other speakers than the virtual microphone at the virtual source 1 location. It is again because the distance between the three reference microphones and speaker 1 is larger than the distance between the virtual source location and speaker 1.

As shown in this section, the proposed procedure using the array microphones for the prediction of the virtual source signals is innovative in that (1) it does not require

time-consuming, labor-intensive, surface-flush-mounted microphone installation, enabling to evaluate the aeroacoustic noise performance of a large number of automobiles effectively and (2) it can potentially result in the highly selective separation of aeroacoustic source signals by predicting the virtual source signals much closer to real source locations than real surface mounted microphones.

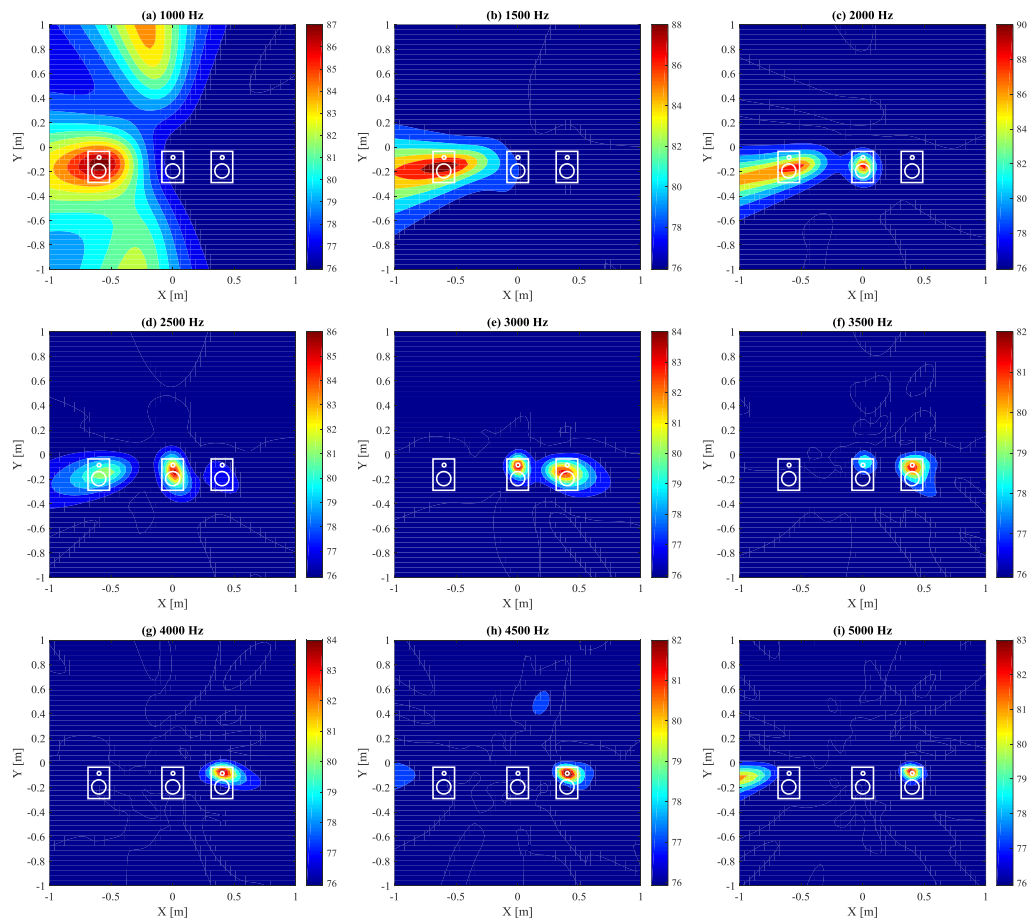


Figure 24: MUSIC beamforming powers on the front of the three speakers at different frequencies: (a) 1 kHz, (b) 1.5 kHz, (c) 2 kHz, (d) 2.5 kHz, (e) 3 kHz, (f) 3.5 kHz, (g) 4 kHz, (h) 4.5 kHz, and (i) 5 kHz. Notes that white lines in the plot show the locations of the speakers, and speaker units.

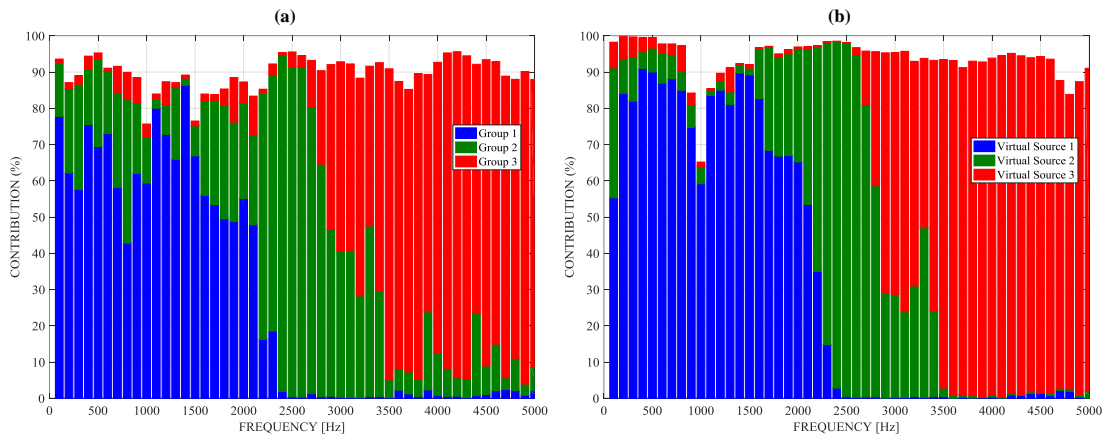


Figure 25: Contribution analysis results obtained with real and virtual source signals: (a) Real source signals measured by using real reference microphones and (b) Virtual source signals reconstructed by using measured array microphone signals.

8. CONCLUSIONS

In this thesis, the contribution analysis method based on the Cholesky Decomposition (CD) is proposed to decompose the measured interior noise spectra in an automobile into physically meaningful, uncorrelated contributions of the external aeroacoustic noise sources. An experiment with two speakers driven by two independent white noise sources was conducted for the validation of the proposed method. Through the two speaker experiment, it is shown that the contribution of both speakers is successfully decomposed: each contribution can be associated with the noise radiated from one of the speakers.

The automobile test at the two traveling speeds, 65 mph and 80 mph, was conducted with 64 exterior microphones and 4 interior microphones. From the contribution analysis results of the experimental data, the first nine highest contributions to the interior noise were observed at the microphone groups of the upper area of the front left window, the upper area of the front right window, the lower area of the front left window, the hood, the lower area of the front right window, the lower area of the rear right window, and the upper area of the rear right window. The aeroacoustic noise with high contributions at the windows may be dominantly generated from the side mirrors and the A-pillars. Through the comparisons of the automobile contribution analysis results, it was shown that the contribution of the windows increased when the vehicle speed increased. Regarding the effects of the seat position on the contribution, the higher contribution could be obtained from the window closer to the specific seat of interest.

The microphone-array-measurement-based contribution analysis procedure was validated by conducting the experiment with three speakers driven by the independent source signals. In the near future, this procedure will be used to evaluate a large number of aeroacoustic automobile designs since it does not require the time-consuming and labor-intensive installation of the surface-flush microphones.

REFERENCES

- [1] S. K. Jha, "Characteristics and sources of noise and vibration and their control in motor cars," *Journal of Sound and Vibration*, vol. 47, no. 4, pp. 543-558, 1976.
- [2] D. Tcherniak and A. P. Schuhmacher, "Application of decomposition-based technique in NVH source contribution analysis," in *Proceedings of the International Conference on Noise and Vibration Engineering (ISMA)-2008*, Leuven, Belgium, 2008.
- [3] J. S. Bendat, "System identification from multiple input/output data," *Journal of Sound and Vibration*, vol. 49, no. 3, pp. 293-308, 1976.
- [4] J. S. Bendat and A. G. Piersol, "Random data: Analysis and measurement procedures," in *Third Edition*, Hoboken, NJ, John Wiley & Sons, 2000, pp. 240-271.
- [5] J. Y. Chung, M. J. Crocker and J. F. Hamilton, "Measurement of frequency responses and the multiple coherence function of the noise-generation system of a diesel engine," *Journal of the Acoustical Society of America*, vol. 58, pp. 635-642, 1975.
- [6] A. G. Gonzalez, J. Rodriguez, X. Sagartzazu, A. Schuhmacher and I. Isasa, "Multiple coherence method in time domain for the analysis of the transmission paths of noise and vibrations with non-stationary signals," in *Proceedings of the*

- International Conference on Noise and Vibration Engineering (ISMA) 2010*,
Leuven, Belgium, 2010.
- [7] D. d. Klerk and A. Ossipov, "Operational transfer path analysis: Theory, guidelines and tire noise application," *Mechanical Systems and Signal Processing*, vol. 24, no. 7, pp. 1950-1962, 2010.
- [8] K. Wyckaert and H. V. d. Auweraer, "Operational analysis, transfer path analysis, modal analysis: Tools to understand road noise problems in cars," No. 951251, SAE Technical Paper, 1995.
- [9] J. Plunt, "Finding and fixing vehicle NVH problems with transfer path analysis," *Sound and Vibration*, vol. 39, no. 11, pp. 12-17, 2005.
- [10] P. Gajdatsy, K. Janssens, L. Gielen, P. Mas and H. V. D. Auweraer, "Critical assessment of operational path analysis: Effect of coupling between path inputs," *Journal of the Acoustical Society of America*, vol. 123, no. 5, pp. 3876-3876, 2008.
- [11] J. Putner, M. Lohrmann and A. Kaltenhauser, "Operational transfer path analysis predicting contributions to the vehicle interior noise for different excitations from the same sound source," in *Proceedings of Inter-Noise 2012*, New York City, NY, United States, 2012.
- [12] N. B. Roozen, Q. Leclere and C. Sandier, "Operational transfer path analysis applied to a small gearbox test set-up," in *Proceedings of Acoustics 2012*, Nantes, France, 2012.

- [13] J. Putner, M. Lohrmann and H. Fastl, "Contribution analysis of vehicle exterior noise with operational transfer path analysis," in *Proceedings of Meetings on Acoustics (ICA) 2013 Montreal*, Montreal, Canada, 2013.
- [14] W. Liu and D. J. Ewins, "Transmissibility properties of MDOF systems," in *Proceedings – SPIE the International Society for Optical Engineering*, San Jose, CA, United States, 1998.
- [15] P. S. Varoto and K. G. McConnell, "Single point vs. multi point acceleration transmissibility concepts in vibration testing," in *Proceedings of the 16th International Modal Analysis Conference (IMAC XVI)*, Santa Barbara, CA, United States, 1998.
- [16] A. M. R. Ribeiro, "On the generalization of the transmissibility concept," in *Proceedings of NATO/ASI Conference on Modal Analysis and Testing*, Sesimbra, Portugal, 1998.
- [17] N. M. M. Maia, J. M. M. e. Silva and A. M. R. Ribeiro, "The transmissibility concept in multi-degree-of-freedom systems," *Mechanical Systems and Signal Processing*, vol. 15, no. 1, pp. 129-137, 2001.
- [18] M. Fontul, A. M. R. Ribeiro, J. M. M. e. Silva and N. M. M. Maia, "Transmissibility in structural coupling," in *Proceedings of the International Conference on Noise and Vibration Engineering (ISMA)*, Leuven, Belgium, 2004.
- [19] N. M. M. Maia, M. Fontul and A. M. R. Ribeiro, "Transmissibility of forces in multiple-degree-of-freedom systems," in *Proceedings of the International*

- Conference on Noise and Vibration Engineering (ISMA 2006)*, Leuven, Belgium, 2006.
- [20] D. Tcherniak, "Application of transmissibility matrix method to structure borne path contribution analysis," in *Proceedings of German Annual Conference on Acoustics (NAG/DAGA 2009)*, Rotterdam, Holland, 2009.
- [21] D. Tcherniak and Y. S. Ryu, "Developments in transmissibility matrix method in application for structure borne noise path analysis," in *Proceedings of Society of Automotive Engineering of Japan (JSAE) 2009*, Yokohama, Japan, 2009.
- [22] H.-S. Kwon, Y.-J. Kim and J. S. Bolton, "Compensation for source nonstationarity in multi-reference, scan-based nearfield acoustical holography," *Journal of the Acoustical Society of America*, vol. 113, pp. 350-368, 2003.
- [23] Y.-J. Kim, J. S. Bolton and H.-S. Kwon, "Partial sound field decomposition in multireference near-field acoustical holography by using optimally located virtual references," *Journal of the Acoustical Society of America*, vol. 115, no. 4, pp. 1641-1652, 2004.
- [24] M. Cho, C. Oh, H. G. Kim and K. D. Ih, "On the ability of numerical solvers to predict interior noise transmission of aerodynamic and aeroacoustic sources in a simplified vehicle model," in *Proceeding of Inter-Noise 2015*, San Francisco, CA, United States, 2015.
- [25] L. E. Hunt, R. S. Dowans III, M. S. Kuester, E. B. White and W. S. Saric, "Flow quality measurements in the Klebanoff-Saric Wind Tunnel," in *Proceedings of*

27th AIAA Aerodynamic Measurement Technology and Ground Testing Conference, Anaheim, CA, United States, 2010.

[26] "Klebanoff-Saric Wind Tunnel Facility," 2013. [Online]. Available: <http://kswt.tamu.edu/facility/>. [Accessed 26 09 2016].

[27] P. K. Kundu, I. M. Cohen and D. R. Dowling, "Fluid Mechanics," in *5th Ed.*, Waltham, MA, United States, Academic Press, 2012, p. 391.

APPENDIX

A. Contribution Analysis Software

The Contribution Analysis Software (CAS) was developed by using the Graphical User Interface Development Environment (GUIDE) in MATLAB. Figure A1 shows the main window of the CAS. This software is designed to process new measurement data as well as to reprocess previously processed data. The main functionalities of the CAS are as follows:

- The CAS manages a file referred to as the CAS project file that includes raw time data, experimental parameters, data processing parameters, post-processing parameters for plots or export, and analyzed contribution results.
- The raw time data in the ASCII file format can be imported to the CAS as input data.
- A user can select various data processing parameters including A-weighting, 1/1 or 1/3 octave/linear bands, time window functions, etc.
- The analysis results include individual source contributions, group contributions, and overall contributions.
- The colors and names of reference channels or groups can be selected by a user.
- The groups of reference channels can be selected by a user.
- The analyzed contribution results can be plotted in the software and the plots can be saved as image files.
- The analyzed results can also be exported to ASCII files.

A.1 Description of CAS

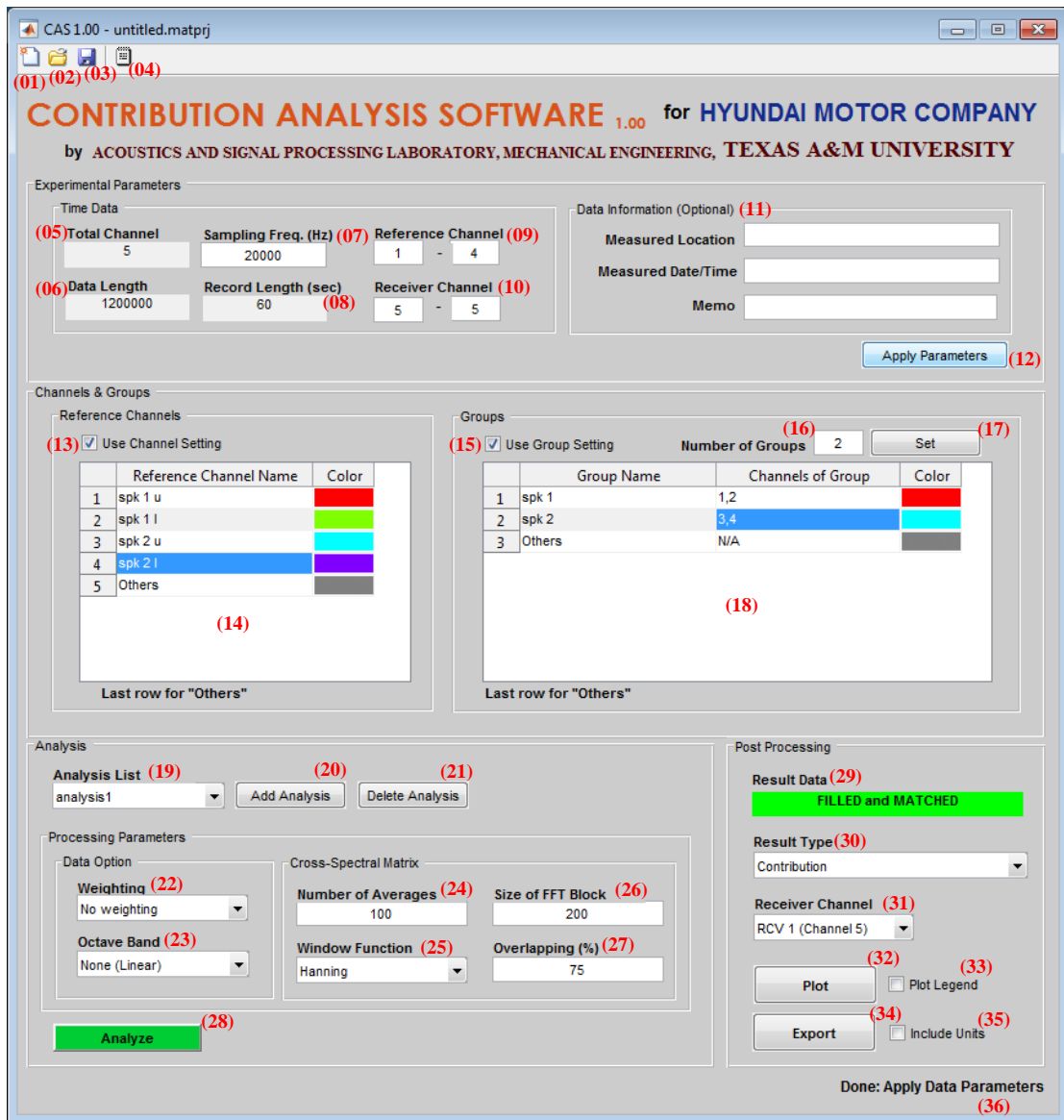


Figure A1: Main window of developed Contribution Analysis Software (CAS).

- (Fig. A1-01) “New Project” button: Create a new project file, all values will be set to defaults.
- (Fig. A1-02) “Open Project” button: Open an existing project file.

- (Fig. A1-03) “Save Project” button: Save current data to the project file. When it is pressed for the first time in a project, it save the project and a user needs to select a path and filename. Once the project is saved, the click of this button will overwrite the opened project file.
- (Fig. A1-04) “Import Time Data” button: Open a popup window to import raw time data in the ASCII file format.
- (Fig. A1-05) “Total Channel” indicator: Show the total number of channels in the loaded time data.
- (Fig. A1-06) “Data Length” indicator: Show the time data length of the loaded time data.
- (Fig. A1-07) “Sampling Freq. (Hz)” input: Input the sampling frequency in Hertz used in the loaded time data. A user has to input the sampling frequency: there is no default value for this input.
- (Fig. A1-08) “Record Length (sec)” indicator: Show the record length in second of the loaded time data.
- (Fig. A1-09) “Reference Channel” inputs: Input start and end channels of the reference sensors. A user has to input these channel numbers.
- (Fig. A1-10) “Receiver Channel” inputs: Input start and end channels of the receiver sensors. A user has to input these channel numbers.
- (Fig. A1-11) “Data Information (optional)” input: Input any descriptive information on the current project.

- (Fig. A1-12) “Apply Parameters” button: Apply the experimental parameters to the current project. Prior to pressing this button, the raw time data has to be imported and the sampling frequency, the reference channels, and the receiver channels have to be filled out. The length of Table of Reference Channels will be changed by the setting of Reference Channel.
- (Fig. A1-13) “Use Channel Setting” checkbox:

Status	Action
Checked	Use the reference channel names and colors in the table for result plots.
Unchecked	Use the default data.

- (Fig. A1-14) Table of Reference Channels:

The last row of the table is for “Others”.

Column	Description
First Column	Reference channel number
Reference Channel Name	Name for each reference channel.
Color	Color for each reference channel. A user can choose a desired color in the color pickup window.

- (Fig. A1-15) “Use Group Setting” checkbox:

Status	Action
Checked	Use the group names and colors in the table below for result plots.
Unchecked	Use the default data.

- (Fig. A1-16) “Number of Groups” input: Number of groups to use.
- (Fig. A1-17) “Set” button for number of groups: Set the length of Table of Groups with Number of Groups.
- (Fig. A1-18) Table of Groups:

The last row of the table is for “Others”.

Column	Description
First Column	Group number
Group Name	Name for each group.
Channels for Group	Reference channels for each group. The channel numbers should be separated with commas. (i.e., channels 1, 2, and 3 are selected for a group, it should be input as "1,2,3").
Color	Color for each group. A user can choose a desired color in the color pickup window.

- (Fig. A1-19) "Analysis List" popup: Show the list of current analysis or analyses.
- (Fig. A1-20) "Add Analysis" button: Add an empty analysis to the analysis list.
- (Fig. A1-21) "Delete Analysis" button: Delete the current analysis in the analysis list.
- (Fig. A1-22) "Weighting" popup:




List	Description
No weighting	No weighting.
A-weighting	Apply A-weighting for the analysis.

- (Fig. A1-23) "Octave Band" popup:

List	Description
None (Linear)	Analyze in linear frequency domain.
1/1 Octave Band	Analyze in 1/1 octave band frequency domain.
1/3 Octave Band	Analyze in 1/3 octave band frequency domain.

- (Fig. A1-24) "Number of Averages" input: Input the number of averages to build a CSM.
- (Fig. A1-25) "Window Function" popup: Show the various time window functions to be applied in the time data.

- (Fig. A1-26) “Size of FFT Block” input: Input the size of FFT block to build the CSM.
- (Fig. A1-27) “Overlapping (%)” input: Input the time data overlapping in percent to build CSM.
- (Fig. A1-28) “Analyze” button: Start to analyze. When it is pressed, the “Abort” button to abort the current data processing will be appeared next to this button.
- (Fig. A1-29) “Result Data” indicator:

Status	Description
EMPTY 	An analyzed result data does not exist.
FILLED but NOT MATCHED 	An analyzed result data exists but its processing parameters do not match with the current ones.
FILLED and MATCHED 	An analyzed result data exists and its processing parameters match with the current ones.

- (Fig. A1-30) “Result Type” popup:

List	Description
Contribution in Percent	Normalized contributions of reference channels in percent
Linearly Scaled Contribution	Linearly scaled Decibel (dB) contributions of reference channels
Overall Contribution	Overall contributions of reference channels
Group Contribution	Normalized contributions of groups in percent
Grouped, Linearly Scaled Contribution	Linearly scaled Decibel (dB) contributions of groups
Grouped, Overall Contribution	Overall contributions of groups

- (Fig. A1-31) “Receiver Channel” popup: Select the Receiver Channel of interest.

- (Fig. A1-32) “Plot” button: Plot the contribution analysis with the selected Result Type (Fig. A1-30) and the selected Receiver Channel (Fig. A1-31).

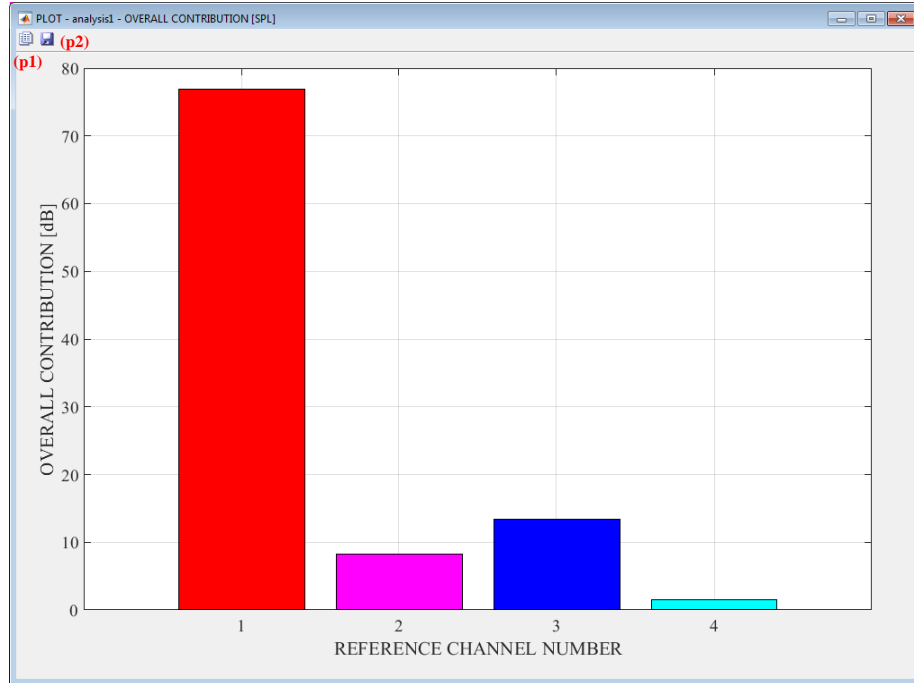


Figure A2: Plot window of CAS.

- (Fig. A2-p1) Copy Figure to Clipboard: Copy the displayed figure to the clipboard.
- (Fig. A2-p2) Save Figure as: Save the displayed figure to an image file. A user can select the image file format.
- (Fig. A1-33) “Plot Legend” checkbox:

Status	Description
Unchecked	Not display the legend in the plot.
Checked	Display the legend.

- (Fig. A1-34) “Export” button: Export the contribution result data of the selected Result Type (A1-30) and Receiver Channel (A1-31) to an ASCII file.

- (Fig. A1-35) “Include Units” checkbox:

Status	Description
Unchecked	Not include the units in the exported data.
Checked	Include the units in the exported data.

- (Fig. A1-36) “Status Message” indicator”: Display several status messages.

A.2 Quick instruction.

- 1) Execute the CAS.
- 2) a) Create a new project (Fig. A1-02), or b) Open an existing project (Fig. A1-03).
- 3) Import a raw time data (Fig. A1-04) when the new project is created in step 2).
- 4) Fill out the experimental parameters (Fig. A1-07, 09, 10, and 11).
- 5) Apply the parameters to the project (Fig. A1-12).
- 6) After successfully applying the parameters, a user can save the current parameters to the project file anytime.
- 7) Fill out the Reference Channel table (Fig. A1-14) and check the “Use Channel Setting” box (Fig. A1-13).
- 8) Input the “Number of Groups” (Fig. A1-16) and press the “Set” button (Fig. A1-17).
- 9) Fill the Group table (Fig. A1-18) and check the “Use Group Setting” box (Fig. A1-15).
- 10) Add an analysis by pressing the “Add Analysis” button (Fig. A1-20).
- 11) Set the “Processing Parameters” (Fig. A1-22, 23, 24, 25, and 26).
- 12) Press “Analyze” button (Fig. A1-28) and wait until it is completed.
- 13) Select the “Result Type” (Fig. A1-30) and “Receiver Channel” (Fig. A1-31) to plot or export the results.
- 14) Press the “Plot” button (Fig. A1-32) to generate a result plot. Copy the plot to the clipboard by pressing the “Copy Figure to Clipboard” button (Fig. A2-p1) or save the plot to an image file by pressing “Save Figure as” button (Fig. A2-p2).
- 15) Export the result data to an ASCII file by pressing the “Export” button (Fig. A1-34).